MESOPOROUS IRON OXIDE ENERGETIC COMPOSITES WITH SLOW BURN RATE, SUSTAINED PRESSURE AND REDUCED ESD SENSITIVITY FOR PROPELLANT APPLICATIONS

MESOPOROUS IRON OXIDE ENERGETIC COMPOSITES WITH SLOW BURN RATE, SUSTAINED PRESSURE AND REDUCED ESD SENSITIVITY FOR PROPELLANT APPLICATIONS

A Thesis
presented to
the Faculty of the Graduate School
at the University of Missouri-Columbia
In Partial Fulfillment
of the Requirements for the Degree

Master of Science

By

Syed Barizuddin

DECEMBER 2006

The undersigned, appointed by the dean of the Graduate School, have examined the thesis entitled

MESOPOROUS IRON OXIDE ENERGETIC COMPOSITES WITH SLOW BURN RATE, SUSTAINED PRESSURE AND REDUCED ESD SENSITIVITY FOR PROPELLANT APPLICATIONS

presented by Syed Barizuddin,

a candidate for the degree of Master of Science, and hereby certify that, in their opinion, it is worthy of acceptance.

Professor Shubhra Gangopadhyay

Professor Rajesh Shende

Professor Tushar K. Ghosh

ACKNOWLEDGMENTS

I have been working with Dr. Shubhra Gangopadhyay for several months now and the experience has been challenging, stimulating and simply stated a lot of hard work. This has been an extremely satisfying and enjoyable time. As part of her team I have come to appreciate the extent of her vast knowledge. She brings an enormous amount of energy and commitment to every project. Her support and guidance have been invaluable. Dr. "G" – your question "show me the results", has been a strong motivator. I aspire to always have results to show.

Dr. Rajesh Shende has been the backbone of this thesis. He has worked with me to sort out problems and figure out solutions all through my research. His knowledge of chemistry has helped me immensely in navigating through the hurdles in my research. His kind and gentle demeanor always helped to calm us when we got frustrated at the lab.

I also extend my gratitude to Dr. Tushar K. Ghosh, Professor, Nuclear Science and Engineering Institute, who was kind enough to be my external advisor at very short notice. Also my thanks and gratitude is due to Dr. Keshab Gangopadhyay for his intuitive and wise advice.

Thanks are also due to Cheryl Jensen and Randy Tindall from the Electron Microscopy core at UMC for helping with the analysis of my samples.

TABLE OF CONTENTS

ABSTRACT

The objective of this thesis is to synthesize a slow burning nanoenergetic formulation of mesoporous iron oxide with sustainable pressure characteristics and reduced electrostatic discharge ignition sensitivity.

The choice of iron oxide is made because its redox reaction with Al-nanoparticles releases energy which is lower as compared with the other redox reactions of CuO, MoO_3, Bi_2O_3, WO_3, etc. with Al-nanoparticles. We attempted to reduce the combustion wave velocity by infiltrating polymers inside porous Fe_2O_3 and combining it with Al-nanoparticles. When such a composite is ignited the polymer does not contribute to the energetic process but, leads to slower combustion velocities. In addition, polymer decomposes into gaseous products upon igniting inside the mesoporous confinements of Fe_2O_3 oxidizer. Due to the longer diffusion length, the composites of polymer modified porous gels mixed with fuel nanoparticles will provide sustainable pressure characteristics. Furthermore, modifications with the polymers can reduce the electrostatic discharge (ESD) ignition sensitivity of nanoenergetic composites.

The composites reported in this thesis will be useful for propellant applications because propellants in general burn at a slow rate and provide pressures in the MPa range sustaining for few milliseconds. Propellant formulations that are currently being investigated contain metal oxide oxidizer and fuel nanoparticles mixed with low grade explosives. Such formulations do not show sustained

pressure characteristics and detonate if explosives are charged above a certain critical mass over the total mass of energetic. Non-explosive formulations containing polymers are currently being explored for propellant applications. This thesis presents the results obtained on the nanoenergetic composites prepared with polymers, which exhibit the desired propellant characteristics.

Acrylamidomethyl cellulose acetate butyrate (AAMCAB) was selected as a candidate to infiltrate the porous Fe_2O_3 gel. The structure of AAMCAB contains many nitrogen and carbon atoms which will produce gaseous species on combustion. Due to the nanosized confinements, these gases will release at a slower rate over the diffusion path length due to the resistance provided by the confined surfaces. This will create a situation of sustained pressure release while combustion is in progress. There is practically no information available on the use of this polymer for pressure development purposes in nanoenergetic materials.

We have also explored carboxyl terminated butadiene-acrylonitrile (CTBN) polymer to coat the Al nanoparticles to reduce the ESD ignition sensitivity. This polymer has several well known applications in coating industries. CTBN is an energetic polymer, which will also contribute to the energy of energetic reaction. Thus, by employing this polymer, it is expected that the extent of energy release from thermite reactions will not be reduced. As CTBN is completely soluble in 2-butanone, it is easier to form a solution of this viscous polymer and hence ease the coating process. It is anticipated that this polymer coating will be uniform so that

the surface charge present on energetic materials will be encapsulated, which will help in reducing the electrostatic discharge (ESD) ignition sensitivity of energetic materials.

This thesis presents synthesis of mesoporous iron oxide gel, infiltration of AAMCAB in porous gels, coating of Al-nanoparticles with CTBN and measurements of energetic properties such as the burn rate, pressure characteristics, and ESD ignition energies.

LIST OF FIGURES

CHAPTER 1

None

CHAPTER 2

CHAPTER 3

CHAPTER 4

CHAPTER 5

LIST OF TABLES

CHAPTER 1

None

CHAPTER 2

CHAPTER 3

CHAPTER 4

CHAPTER 5

CHAPTER 1

INTRODUCTION

Nanoenergetic materials comprise of a metal oxide (oxidizer) mixed with nanosized particulates of metal (fuel) nanoparticles. On ignition these materials undergo an oxidation-reduction reaction resulting in substantial heat release. Mixing the fuel and oxidizer in stoichiometric proportions may maximize the energy density of the mixture, but the overall kinetics of the process still requires the two components to mix at the atomic scale in order for the reaction to take place [1]. The propagation or energy release rate is directly dependent on the homogeneous distribution of the oxidizer and fuel in a nanoenergetic composite [2]. In the mixture of non-porous nanoparticles, the propagation rate follows conduction mechanism. However, in the energetic composite of porous particles, conduction and convection mechanisms play a vital role in energy release.

In general, nanoenergetic materials are sensitive to impact, friction, electrostatic discharge (ESD) etc. Among these sensitivities, ESD ignition sensitivity is of prime importance to these types of energetic materials because it poses concerns for safe handling [3, 4].The literature available for such type of materials in terms of their ESD ignition energy sensitivity is very limited. Efforts have been made to measure the electrostatic discharge ignition energy of various Fe_2O_3 based nanoenergetic composites. Another prime consideration will be to look into the means by which this sensitivity could be reduced.

To reduce ESD ignition sensitivity, polymers will be employed [5]. Different polymers will be used to coat the oxidizer and the fuel. It is our understanding that doing so would help in reducing the surface charge on the oxidizer as well as on the fuel, which will contribute in reducing the ESD sensitivity of the energetic nanocomposites. The use of polymer will have a two fold advantages: first, it will lower the sensitivity of the nanocomposites and second, this polymer coating will reduce the burn rate while giving sustained pressure characteristics.

A synthesis approach to formation of ordered mesoporous Fe_2O_3 gel was developed using surfactant templating approach [6, 7]. It involves the reactions of precursors/chemicals in a solution to produce nanometer-sized particles called "sol". The sols can then be linked to form "gel" with the remaining solution residing in surfactant micelles. Upon removal of surfactant micelles, porous gels can be obtained.

Gels can be in the form of either aerogel or xerogel. Aerogels are highly porous and low density gels. Aerogel starts out as a gel, called alcogel. Alcogels are made by polymerizing an alkoxide with water in a mixing solvent (such as ethanol). The reaction occurs by hydrolysis and water condensation, joining together the alkoxide molecules making the bonds to form oligomers. These oligomers join together and form one giant molecule, which is the solid part of a gel. The matrix in the alcogel is filled with solvent, having tiny little pockets of 5 to 150 nm [8]. This gel is made by drying the alcogel and extracting the liquid from the solid component by super critical CO_2 extraction [9, 33]. The evaporating liquid solvent causes the alcogel's solid component to collapse by capillary

action. This means that after the solvent has been completely removed out of the gel, the gel has collapsed and formed a dense solid that is a very small percentage of the original volume of the gel. This solid is referred to as xerogel, which has low or no porosity.

Previously, the sol-gel method has employed the use of metal alkoxide precursor that readily undergoes catalyzed hydrolysis and condensation to form sol of the metal oxide particles with nanometer dimensions. However, some metal alkoxides are expensive and still others are sensitive to moisture, heat and light making long term storage difficult. Metal salts are thus being used as a precursor in synthesizing the metal oxidizer network with the chemical treatment.

To avoid the difficulties involved the following method was used, which is easy, time saving and cost effective. With the surfactant templating approach it is possible to synthesize mesoporous Fe_2O_3 –based energetic composite [10]. In this process the iron oxide-based porous solids are prepared by Brij-76 (co-polymer) non-ionic surfactant templating approach using Fe (III) salt precursor. The resulting gel is aged and treated with solvent to remove impurities. Then the gel is annealed and characterized by FTIR and TEM analysis to understand the chemical composition and the microstructure. The Fe_2O_3 gels are combined with Al nanoparticles to prepare an energetic composite. The other typical fuels are zirconium, titanium, magnesium and boron. The reaction between different oxidizers and fuels will result in different energy release rates. Typical oxidizers include various nitrates, calcium chromate, lead nitrate, copper oxide, and perchlorates of sodium, potassium and ammonia. The rates depend not only on density, temperature and pressure but are also affected by the porosity, particle size, purity, homogeneity (degree

of mixing) and stoichiometry (fuel or oxidizer ratio). The typical reaction equation is given as [7].

$$Fe_2O_3 + 2Al \longrightarrow 2Fe + Al_2O_3 + \Delta H\ (-425KJ/mol)\ (1)$$

In this reaction the oxide of one metal is reduced and the other metal oxidized. The product in the above chemical reaction acts as a heat transfer medium for specific application. The only gaseous products are vaporized metal and metal oxide from the heat of the reaction which solidifies very fast. The combustion wave velocity and pressure depends on the temperature of combustion and on the number of moles of gas. Since thermites do not have any compounds which can form gaseous products on combustion their pressure is limited. The addition of some compounds capable of producing gaseous products can increase the pressure further. The requirements for choosing such a material for extra gas generation should be that, they should be easily combustible and should not react or interfere with the thermite process. This intended modification was achieved with use of polymers. The purpose of this composite was to achieve propellant characteristics.

Propellants are mixtures of chemical compounds capable of producing large volumes and they give out heat. They also have high energy content and must have defined burning characteristics. The earlier propellant known as “black powder” had serious disadvantages. They were unpredictable in use, developed extremely dirty gases and left hazardous residue. The discovery of nitrocellulose led towards the generation of smokeless powders. The propellants are mainly divided into two classes: Single base (SB) and double base (DB) propellants. The main ingredient of SB is basically

nitrocellulose which is made colloidal by the action of the solvent. DB propellants contain nitroglycerine or other nitroglycol compounds and nitrocellulose [11, 37]. Separate classes of propellants called triple base (TB) propellants are made up of DB propellants with picrite or nitroguanidine added to the formulation [11]. A fourth type, the composite propellant is a more recent development compared with the other two. This is based on an oxidizing solid, commonly a perchlorate, together with an organic binder which acts as fuel and also gives adequate mechanical strength to the resulting propellant. These excellent mechanical properties allow propellant grains to be manufactured in dimensions larger than SB and DB. This and the high energy content of composite propellant make them a material for defense and space use.

The size, dimension and geometry of propellant grains based on SB and DB propellant is limited. For this reason the development of composite propellants began. In the beginning, ingredients used were tar or rubber and an oxidizer. Today, a curable polymeric binder is loaded with oxygen-rich, crystalline solids (mostly perchlorates) and a metal (mainly aluminum).

The two main oxidizing compounds used in composite propellant manufacture are ammonium perchlorate (AP) and ammonium nitrate (AN) [11]. The most frequently used is AP. The salt of perchloric acid is more interesting than the chlorate, because it is stable and safer to handle. The decomposition of this during the burning process leads to white smoke. The white smoke could be reduced by adding substances like magnesium-aluminum alloys or sodium nitrate. But this causes tactical problems. The heat given out

is less than that of nitrocellulose (NC) or nitroglycerine (NG). Because composite propellants must burn for a relatively long time, the burning rate has to be low and hence the high heat is not feasible.

The first fuels used in composite propellants as mentioned earlier were tar or rubber. Later, with the evolution of polymer technology, more modern polymeric fuels were introduced like polymethacrylates or polybutadienes. As the polymer is only partially responsible for reducing the redox reaction in the formulation, some metals are added in the composition. The most popular ones are aluminum, zirconium (high density), beryllium (very energetic but toxic), boron and magnesium.

The velocity of a burning reaction, also called combustion, is given by the steady state of heat production and the efficiency of heat transfer to reach ignition temperature within a material. The combustion of this material is linked to the superficial pyrolysis reaction of the constituents. This reaction produces gases which react with each other producing flames with high temperature. Addition of special materials will influence the propellant burning rate, pressure characteristics and reduce the sensitivity of the propellant.

For the formulation used in this study, both the oxidizer (Fe_2O_3 gel) and the fuel (Al-nanoparticles) were modified with the polymer to manipulate propellant characteristics ESD sensitivity. The nanoenergetic composites prepared has slower burn rates, sustained pressure characteristics and reduced ESD ignition sensitivity.

Chapter 2 deals with the synthesis and characterization of mesoporous Fe_2O_3 gel. The method employed in the synthesis is user friendly, cost effective and simple. It describes the removal of impurities with solvent treatment. This chapter also provides the results obtained on impurity removal, Fe_2O_3 phase formation and conversion with respect to precursor usage. Results obtained on FTIR and TEM analysis are presented in this chapter.

Chapter 3 deals with the infiltrating polymer inside the porous oxidizer. It also describes the methods for coating of Al nanoparticles with an energetic polymer. The metal fuel of Al and Fe_2O_3 oxidizer are in contact with each other. At the point of contact a hot spot is generated. When non-energetic polymer is used, it acts like a heat sink and will not propagate. Instead if energetic polymer is used, hot spot density is maintained which in turn provide sustained energy for the combustion wave front. Furthermore, it describes the process of separating coated Al-particles from uncoated particles.

Chapter 4 describes the methods of combining polymer impregnated oxidizers with the Al-nanoparticles. This chapter presents the results obtained on the burn rate and pressure characteristics of various Fe_2O_3 -based energetic composites.

Chapter 5 presents the results obtained on ESD ignition energy of Al-nanoparticles, polymer coated particles, and nanoenergetic composites are presented in this chapter.

Conclusion

Future Work

CHAPTER 2

SYNTHESIS OF MESOPOROUS Fe_2O_3 GEL AND IT'S CHARACTERIZATION

2.1 Introduction:

The sol-gel method has provided a very important means of preparing inorganic oxides. It is a wet chemical method and a multi-step process involving both chemical and physical processes such as hydrolysis, polymerization, drying and densification [12]. Porous oxidizer can be easily prepared using the sol-gel approach. In general, this process involves the formation of a solid phase, the sol, which consists of a colloidal suspension containing solid particles of a diameter of a few hundred nanometer suspended in a liquid phase. The gelation of the same produces a new phase (the gel) by condensation or, polymerization of the particles to generate a solid macromolecule immersed in a liquid phase (solvent). Removal of the liquid phase results in a porous solid matrix.

To achieve ordered arrangement of pores and uniform pore size distribution, surfactant templating method is very effective [12]. Surfactant micelles self-assemble in a solution and produce a template with uniform micelles distribution. When inorganic oxidizer precursor is introduced in a solution, it goes around the micelles template. Removal of the template leaves behind the imprints of inorganic oxidizer network with pores in place of micelles. Therefore, by using surfactant templating method, an oxidizer with ordered pore distribution and uniform pore sizes can be easily achieved. Recently, synthesis of mesoporous Fe_2O_3 using surfactant templating method was reported [12, 28, 31, 38]. The other methods of interest to prepare nanoporous Fe_2O_3 could be the aerogel process, aero-sol-gel synthesis etc. In aerogel synthesis of Fe_2O_3, the gel is prepared using normal sol-

gel method and subjected to the supercritical fluid. The role of supercritical fluid is to extract solvent from the gel leaving the pores behind. Aero-sol-gel synthesis of nanoporous Fe_2O_3 particles involved the addition of precursor directly into a gas-phase followed by gas-phase polymerization or condensation [12].

In the synthesis of mesoporous Fe_2O_3 [12, 29, 32], precursors such as Fe (III)-ethoxide, $FeCl_3$ etc. have been used by researchers. Among these, Fe (III)-ethoxide was used with a templating of cetyltrimethylammonium bromide (CTAB) surfactant [12, 26]. In this method, a precipitate was obtained instead of gel, which on solvent extraction and calcination yielded a microstructure with non-uniform distribution of pores of 3-5 nm size. The calcination process involves heating of the finely ground material at high temperatures, to remove the chemically-bound water and/or, surfactant. In the method using $FeCl_3$ precursor, propylene oxide or epichlorohydrin was used as proton scavenger to achieve nanoporous Fe_2O_3 with 2-3 nm pores. However, no ordering of the pores was observed in the microstructure reported for aero-sol-gel synthesis of mesoporous Fe_2O_3 particles. Recently, sol-gel synthesis of Fe_2O_3 from Fe (III)-nitrate precursor using propylene oxide as proton scavenger and Brij-76 as a surfactant was reported [12, 33].

Standard practices suggest that the gels be aged at room temperature in air followed by annealing at various temperatures to remove the liquid phase from the sample. This process results in bringing the micron sized particles closer due to the evaporation of water. Rapid annealing process in air can result in collapse of the pores and this method may not be suitable for making nanoporous Fe_2O_3. Hence the annealing rate should be

reduced to about 1°C/min or slower to prevent the pores from collapsing. Secondly, since the hydrocarbons are removed by decomposition at elevated temperatures, the residues remain in the sample and thus contaminate the sample. At elevated temperatures, there is a possibility of the organic species reacting with the polymerized Fe_2O_3 network thus forming by-products which are not desirable and could be detrimental to energetic properties.

Solvents like ethanol, methanol, and acidic solution of dimethyl ether can dissolve the organic species and still keep the pore boundaries intact [13]. The organic species once dissolved remains in the solution and can be removed easily by filtration. This method has an advantage over the annealing method as this method will remove all impurities while preserving the pore structure.

2.2 Experimental:

2.2.1 Preparation of mesoporous Fe_2O_3 gel: 3.57 gms of Brij 76 (non-ionic surfactant from Sigma Aldrich) is dissolved in 150 ml of 200 proof ethanol. The solution was heated to 60^{o}C and maintained for 20 minutes under constant stirring. 50.0 gms of Fe $(NO_3)_3.9H_2O$ (iron (III) nitrate nonahydrate, 98%, A.C.S. Reagent from Sigma-Aldrich, WI) was dissolved in 275 ml of 200 proof (Ethyl Alcohol USP Absolute -200 Proof from AAPER) ethanol. This solution is placed in a sonicator bath for about 20 minutes to ensure complete dissolution of the salt in ethanol. The solution of 50.0 gms of Fe $(NO_3)_3.9H_2O$ dissolved in 275 ml of (200 proof) ethanol was added to the solution of Brij 76 in ethanol under constant stirring for 15 min. To this solution mixture, 259 ml of the

propylene oxide (reagent grade, 99%, from Sigma Aldrich) was added under constant stirring. On addition of propylene oxide, the solution transforms into a gel of FeOOH (Fe-oxyhydroxide) in 4-5 min.

2.2.2 Solvent extraction: FeOOH gel samples were further processed with ethanol to remove the impurities. In this treatment, the gel was soaked in ethanol for 48 hrs at 60^{o}C under constant stirring. After the solvent treatment, the solution was allowed to stand for a few minutes so that the gel sediments and the ethanol could be decanted. A fresh stock of ethanol (500 ml) is added to the gel and the solution was stirred and again was allowed to stand for some more time. This process was repeated several times until the decanted solution was free of any color. This indicated that the gel was free of impurities. The gel was then heated at 90-95ºC overnight to evaporate the solvent and annealed at 400^{o}C in Thermolyne furnace overnight. A heating cycle of initial ramp rate of 1ºC/min followed by a hold of 12 hrs at 400^{o}C and subsequent cooling to room temperature was used.

2.2.3 Dispersion in hexane using K-sperse dispersing agent: The gel obtained is slightly harder and this hardness can inhibit homogenous mixing with fuel nanoparticles. Therefore, Fe_2O_3 gel (1.0 gms) was placed in 10 ml of hexane and 2-5 mg of K-sperse, a dispersant was added into it. This solution was sonicated for 6-12 hrs and dried at 80ºC to remove the solvent.

2.2.4 Characterization FeOOH / Fe_2O_3:

2.2.4.1 Fourier transform infrared spectroscopy (FTIR): The Fe_2O_3 gel samples were analyzed by ThermoNicolet FTIR to analyze the surface of materials, their chemical constitution and impurities [25]. To prepare sample for FTIR analysis, the gels were dispersed in 2-propanol for 5 min, spin coated on a silicon wafer and dried at 90 ^oC for 10 minutes. The samples were characterized using the total number of scans of 1024 with resolution of 8 cm^{-1}.

2.2.4.2 Transmission Electron Microscopy (TEM): Microstructure analysis of the gel samples was performed using TEM, JEOL 1200 EX, to understand pore size and ordering of the mesopores.

2.3 Results and Discussion:

In the reaction route chosen**,** Fe (III) $(NO_3)_3.9H_2O$ produce $[Fe(OH_2)_6]^{3+}$ complex in presence of C_2H_5OH with the liberation of water molecules and the $(NO_3)^{--}$ species. $[Fe(H_2O)_6]^{3+}$ species (hexa aquairon (III) ion) are highly unstable and undergo reversible reaction with water to produce dimer (reaction 2) [14] . The added propylene oxide scavenges protons (reaction 3) which upon further hydrolysis produce *α*-FeOOH (ferrihydrite). When two FeOOH molecules combine, α-Fe_2O_3 is generated with the liberation of a water molecule [14]. Overall reaction sequence for the hydrolysis of Fe (III) ion and proton scavenging action of propylene oxide are summarized below.

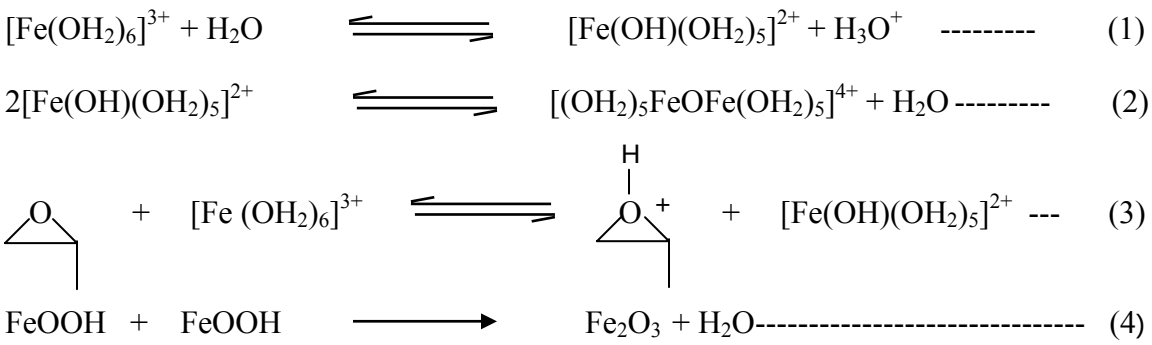

$[Fe(OH_2)_6]^{3+} + H_2O \rightleftharpoons [Fe(OH)(OH_2)_5]^{2+} + H_3O^+$ --------- (1)

$2[Fe(OH)(OH_2)_5]^{2+} \rightleftharpoons [(OH_2)_5FeOFe(OH_2)_5]^{4+} + H_2O$ --------- (2)

$+ [Fe(OH_2)_6]^{3+} \rightleftharpoons + [Fe(OH)(OH_2)_5]^{2+}$ --- (3)

$FeOOH + FeOOH \longrightarrow Fe_2O_3 + H_2O$---------- (4)

FTIR spectra of FeOOH gels prepared using Brij-76 templating is shown in Figure 2.1. In this FTIR spectrum, the presence of –CH vibrations at around 2930 cm^{-1} suggests presence of organic impurities and broad stretching vibration of -OH peak around 3000-3600 cm^{-1} implies the presence of the water in the sample. The peak at around 1630 cm^{-1} is the bending mode of the water in the sample. The absorption peaks around 800 cm^{-1} to 1500 cm^{-1} are associated with the solvent (C_2H_5OH) used, residual propylene oxide or by-products of the ring opening reaction of propylene oxide. The broad absorption peak around 500-700 cm^{-1} can be associated with the Fe-O linkages. The FTIR spectra shown of calcined Fe_2O_3 reveal removal of surfactant and water impurities and the presence of Fe-O vibrations.

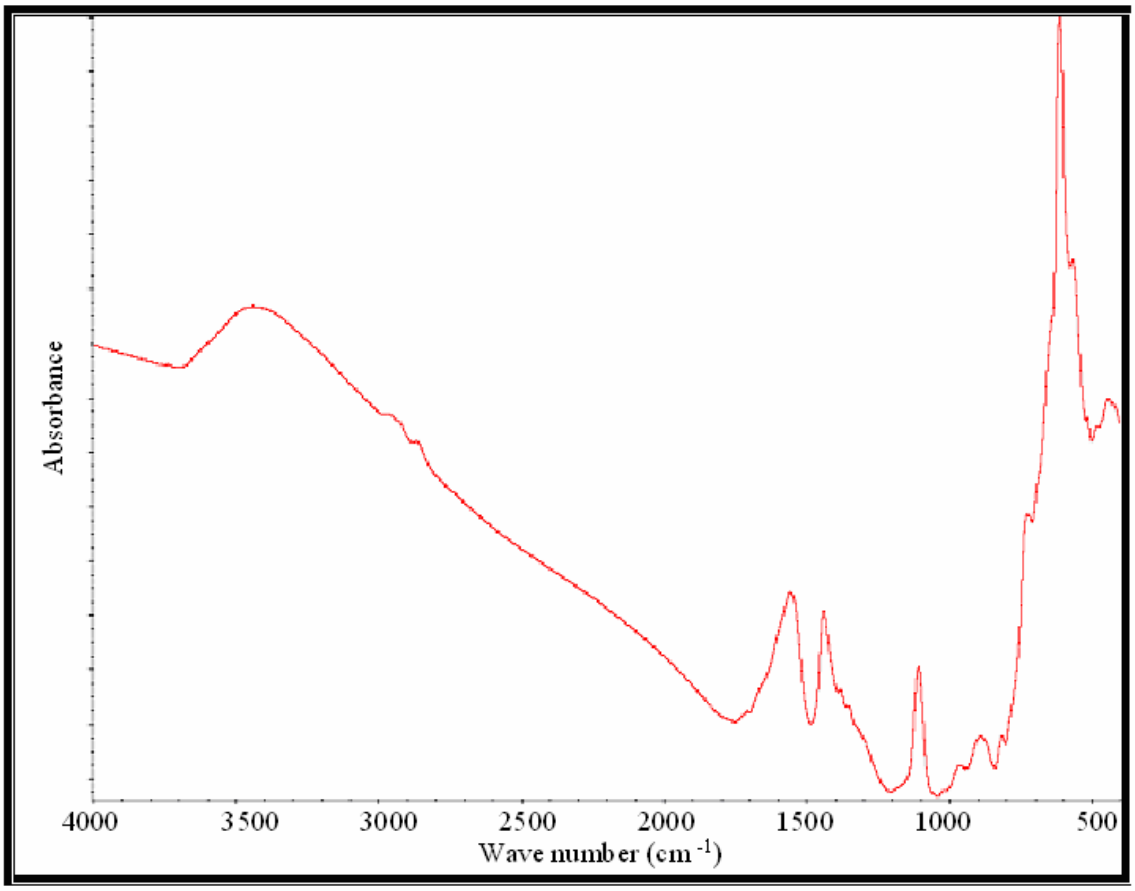

Figure 2.1: FTIR spectra of FeOOH gel

Peaks	Wave number, cm^{-1}	Assignments
1	2930	C-H stretch
2	1610	N-H bend
3	1420	C-H scissoring and bending
4	1120	C-O stretch
5	570	FeO

Table 2.1: Characteristics bond assignment in FTIR spectra of Fe_2O_3

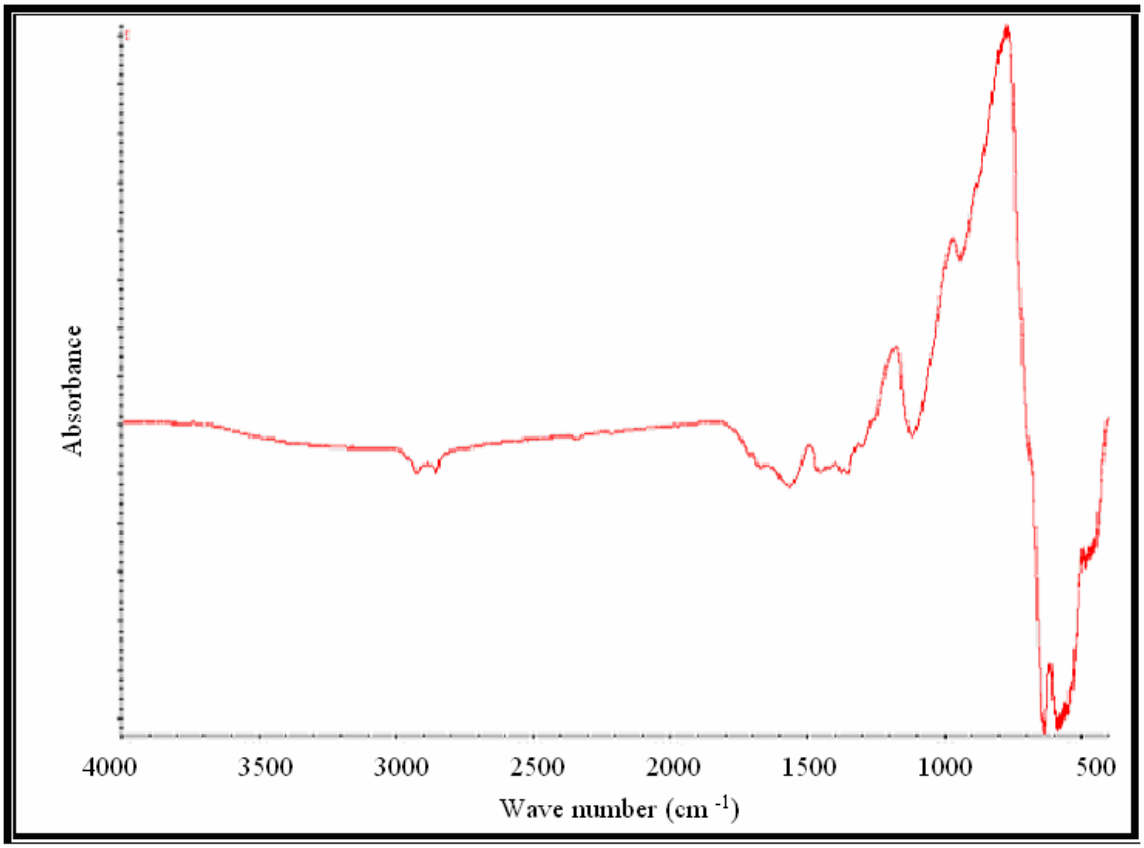

Figure 2.2: FTIR spectra of calcined FeOOH gel

Peaks	Wave number, cm^{-1}	Assignments
1	1470	C-H scissoring and bending
2	1120	C-O stretch
3	780	C-H bend
4	640	C-H bend
5	570	FeO

Table 2.2: Characteristic bond assignment in calcined FTIR spectra of Fe_2O_3

The time required for FeOOH gelation to take place at one particular concentration ratio of Fe (III) $(NO_3)_3.9H_2O$, brij-76, C_2H_5OH and propylene oxide is 1-4 minutes. The amount of precursor, surfactant, acid scavenger, gel times and yields are summarized in table 2.3.

Amount of precursor, surfactant, and acid scavenger used	**Final yield, gms**	**Time to gel**
0.357 gms of Brij 76+5.0 gms of Fe $(NO_3)_3.9H_2O$+50 ml ethanol + 25.9 ml of the propylene oxide	0.357	1-2 min
3.57 gms of Brij 76+50.0 gms of Fe $(NO_3)_3.9H_2O$+500 ml ethanol+ 259 ml of the propylene oxide	7.20	3-4 min

Table 2.3: Time for Fe_2O_3 gel formation and yield of calcined Fe_2O_3 gel

One of the problems encountered during calcination is densification. Rapid annealing process can densify Fe_2O_3 and reduce the porosity. Therefore the annealing process was slowed down by controlling the ramping rate to 1ºC/min.The ferrihydrite gels made with Brij76 as a templating agent were first treated with the solvent to remove impurities and annealed at temperatures of 400ºC for 8 hrs with ramp rate of 1ºC/min [15]. TEM image of calcined Fe_2O_3 gel is shown in figure. 2.3 indicates pore size of about 5-10 nm and organization of the mesopores.

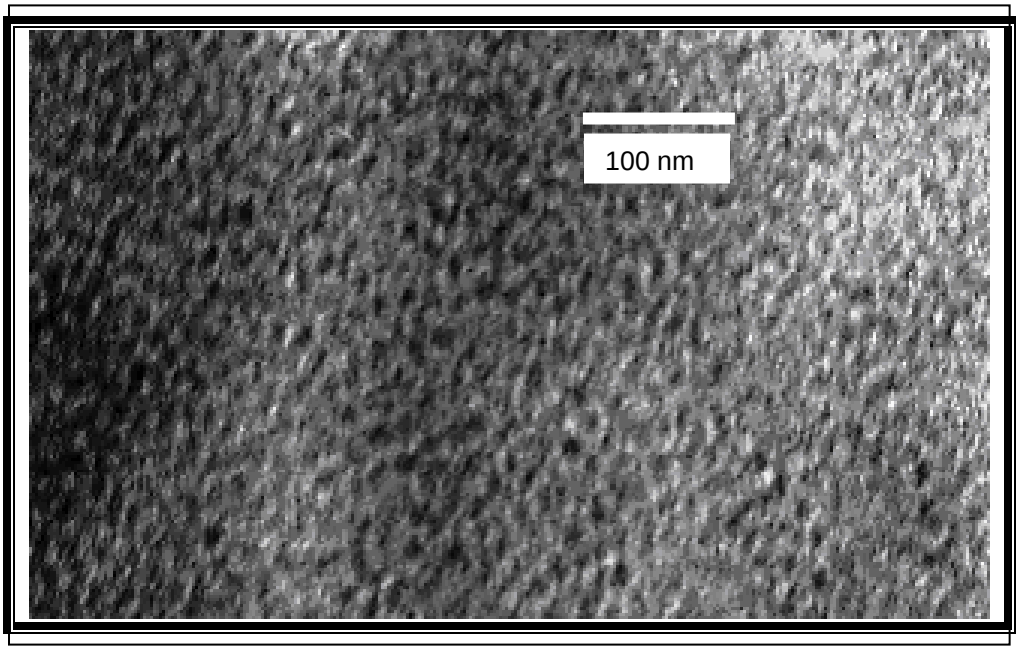

Figure 2.3 TEM of solvent treated and calcined Fe_2O_3 gel

CHAPTER 3

MODIFICATION OF MESOPOROUS Fe_2O_3 WITH POLYMER AND AMMONIUM NITRATE

3.1 Introduction:

Thermite reactions are mostly gas-less combustion processes. As the adiabatic combustion temperatures are about 3000 K, it is possible that at such high temperatures the products of the thermite reactions can produce gaseous species. This will generate some gas pressure. Air entrapped within these confined spaces will lead to gas pressure on combustion. We believe that if polymers are combined with thermites, the gas pressure can still be increased. To verify this, we selected a representative polymer candidate known as acrylamidomethyl cellulose acetate butyrate. Chemical structure of this polymer is presented in figure 3.1. This polymer (AAMCAB) has several carbon and nitrogen atoms, which will combine with oxygen to produce gases on combustion. Also this polymer will decompose into several products that can contribute to higher pressure. AAMCAB has glass transition temperature of 118°C and density of 1.31 g/cc at 25 °C and it is completely soluble in solvents such as acetone, butanone etc [16].

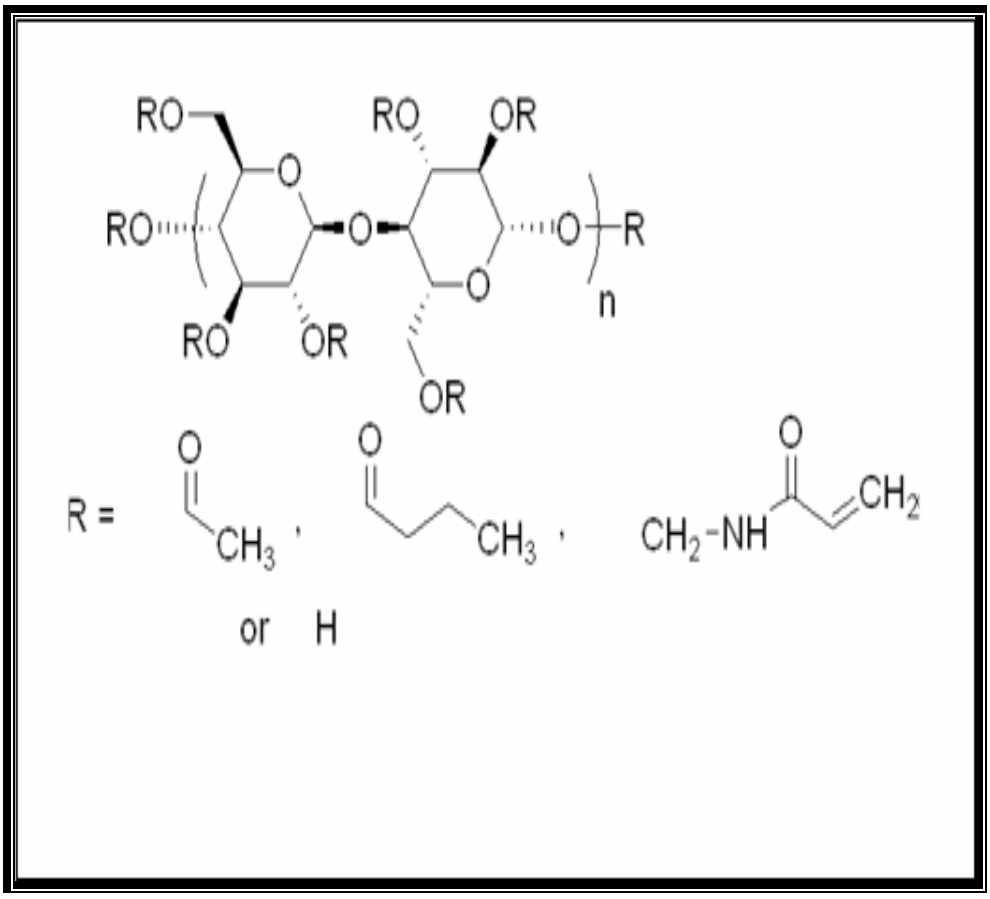

Figure 3.1: Chemical structure of acrylamidomethyl cellulose acetate butyrate [16]

The other type of polymer that we selected to coat the nanoparticles is carboxyl terminated butadiene-acrylonitrile (CTBN) binder. This is an acrylonitrile energetic binder from the family of reactive liquid polymers. These CT (carboxyl terminated) products is a long chain dicarboxylic group. The carboxyl terminated reactive liquid polymers provides durability and it is used in structural automotive and aerospace adhesives, composite bonding/composites matrix resin and coating purposes. The properties of this polymeric binder are listed in table 3.1.

Parameter	Carboxyl terminated polymer, CTBN
Acrylonitrile content, %	10
Acid number	28
mPa•s @ (81°F)	60,000
Solubility arameter	8.46
Specific gravity, (77°F)	0.924
Functionality	1.9
Molecular weight, Mn	3,800
Glass transition temp Tg,°C	–66
Company	Sigma Aldrich

Table 3.1: Physical and thermal properties of CTBN binder [16]

3.2 Experimental

3.2.1 Synthesis of AAMCAB modified mesoporous Fe_2O_3 oxidizer: AAMCAB was obtained from Aldrich, and used as received. It was dissolved in acetone to prepare a solution of 2.5-5% (w/v). To this solution, Fe_2O_3 was added and the mixture was sonicated for 2 hrs and left undisturbed for 12 hours. After that, the mixture was dried at about 80ºC to remove the solvent.

3.2.2 CTBN coating of Al-nanoparticles: To 100 ml of 2-butanone 10.0 gms of CTBN binder was added. This solution was gently heated to dissolve the binder. When the binder was completely dissolved a light yellow colored solution was formed. To this

solution a drop of K-sperse 152 (zinc alkylaryl sulfonate ethylene glycol mono butyl ether), a dispersant was added. A measured quantity of Al-nanoparticles was added to achieve 2.5% and 5% (w/v) of CTBN loadings. The mixture was sonicated for 12 hrs to ensure dispersion of most of the Al- particles. This was heated at about 80ºC to evaporate the solvent. The figure.3.2 shows the final product obtained.

Figure.3.2: Al-nanoparticles coated with CTBN

The use of CTBN energetic polymer helps to maintain the hot spot density which in turn provides sustained energy for the combustion wave front. This is because the metal fuel Al and Fe_2O_3 oxidizer are in contact with each other and at the point of contact a hot spot

is generated. When non-energetic polymer is used, it acts like a heat sink and will not propagate. Hence the use of CTBN will be very effective to obtain propellant characteristics.

3.2.3 Modification of Fe_2O_3 gel with Ammonium nitrate: Ammonium nitrate (reagent grade, Fisher) was used to impregnate the nanoporous Fe_2O_3. 50 mg of ammonium nitrate was dissolved in DI water to which a small quantity of 2-propanol was added. This solution was sonicated until all the ammonium nitrate dissolves. To this solution 120 mg of Fe_2O_3 was added. The flask containing this mixture was covered with a foil and left on a hot plate at 60ºC overnight with constant stirring. The stirrer RPM was maintained at 300. After 24 hrs, the solution was decanted and solids were filtered and washed with ethanol to remove excess ammonium nitrate. The washed solids were dried between 100-120ºC to remove the solvent.

3.3. Mechanism of polymer stabilization and binding:

In this study we use steric stabilization to pacify the nanoparticles and the composite. Steric stabilization, also called polymeric stabilization is a method widely used in stabilization. Though it is less well understood as compared with electrostatic stabilization method, polymeric stabilization offers several advantages over electrostatic stabilization:

- It is a thermodynamic method, so that the particles are always re-dispersible
- A very high concentration can be accommodated, and the dispersion medium can be completely depleted.

- It is not electrolyte sensitive
- It is suitable to multiple phase systems

Compared to electrostatic stabilization mechanism, polymeric stabilization offers an additional advantage in the synthesis of nanoparticles, particularly when narrow size distribution is required. The Polymer layer adsorbed on the surface of nanoparticles serve as a diffusion barrier to the growth species, resulting in a diffusion-limited growth in the subsequent growth of nuclei. Diffusion-limited growth would reduce the size distribution of the initial nuclei, leading to monosized nanoparticles [17]. The dual function of the polymeric layer on the surface of nanoparticles explains the reason why steric stabilization is widely used in the synthesis of nanoparticles.

The solvents in polymers also play an important role. Basically solvents can be grouped into aqueous solvent, which is water, H_2O, and non-aqueous solvents or organic solvents. Solvents can also been categorized into protic solvents, which can exchange protons and examples of which include: methanol, CH_3OH, and ethanol, C_2H_5OH, and aprotic solvents, which can't exchange protons, such as benzene, C_6H_6 [17] . Not all polymers dissolve in solvents and those that are non soluble cannot be used for the steric stabilization. When a soluble polymer dissolves in a solvent, the polymer interacts with the solvent. Such interactions vary within the system as well as with the temperature. For a given system, i.e., a given polymer in a given solvent is dependent on the temperature. At high temperatures, polymer expands, whereas at low temperatures, polymer collapses.

Depending on the interaction between polymer and solid surface, polymers can be grouped into:

1. Anchored polymer, which irreversibly binds to solid surface by one end only, and typically is a diblock polymer **(**Figure 3.3A).
2. Adsorbing polymer, which adsorbs weakly at random points along the polymer backbone (Figure 3.3B).
3. Non-adsorbing polymer, which does not attach to solid surface and thus does not contribute to polymer stabilization.

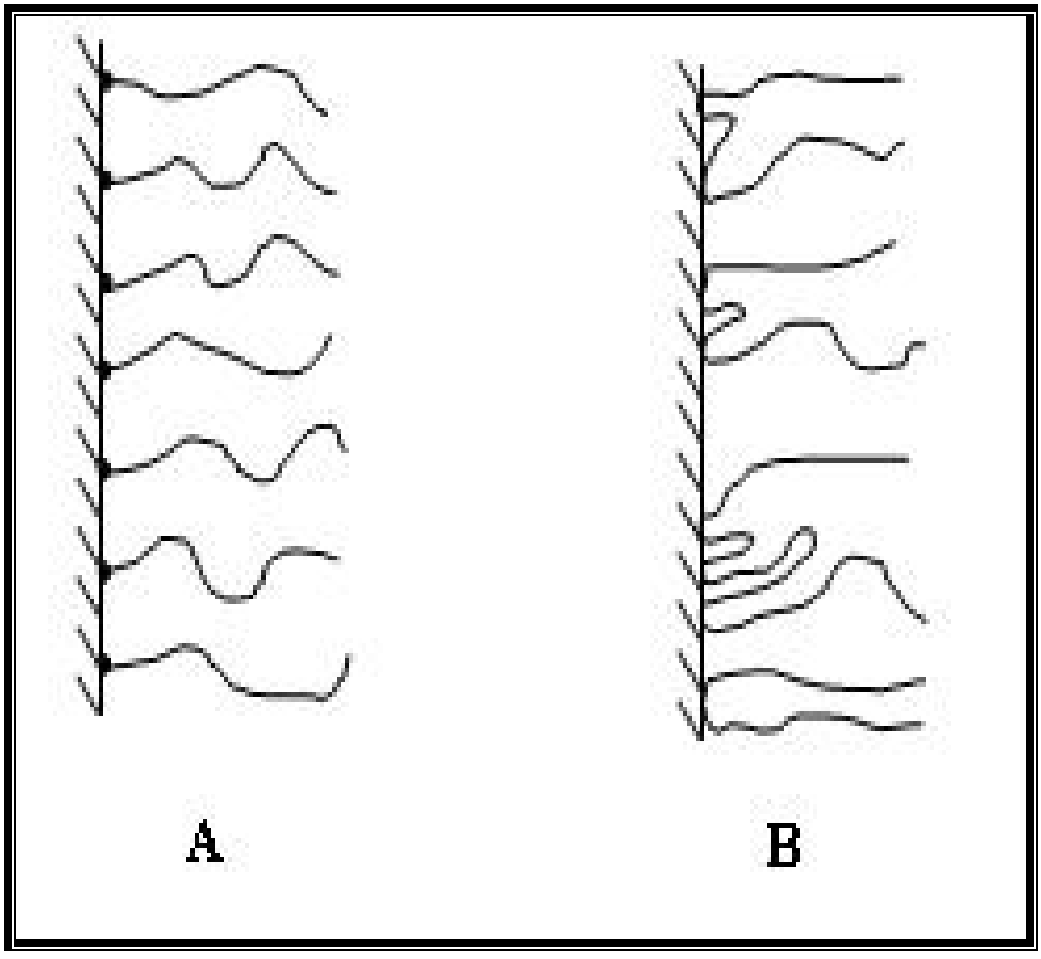

Figure 3.3: A) Anchored Polymer and B) Adsorbing Polymer [17]

The interaction between polymer and solid surface are limited to adsorption of polymer molecules on the surface of the solid. The adsorption can be either by forming chemical bonds between surface ions or atoms on the solid and polymer molecules or by weak physical adsorption. Furthermore, there is no restriction whether one or multiple bonds are formed between the solid and the polymer. No other interactions such as chemical reactions or further polymerization between polymer and solvent or between polymers are considered for the current discussion.

Interactions between polymer layers between two solid particles covered with terminally anchored polymers is schematically illustrated in figure 3.4 A. When two particles approach one another, the attached polymers interact only when the separation distance, H, between the surfaces of two particles is less than twice the thickness, L, of polymer layers. Beyond this distance, there is no interaction between two particles and their polymer layers on surfaces. However, when the distance reduces to less than 2L, but still is larger than, L, there will be interactions between the solvent and the polymer and between the two polymer layers. But there is no direct interaction between the polymer layer of one particle and the solid surface of the opposite particle. In a good solvent, in which the polymer expands, if the coverage of polymer on the solid surface is not complete, particularly less than 50% coverage, when the concentration of polymer in the solvent is insufficient, two polymer layers tend to interpenetrate so as to reduce the available space between polymers. Such an interpenetration of two polymer layers of two approaching particles would result in a reduction of the freedom of polymers, which leads to a reduction of entropy, i.e., $\Delta S < 0$. As a result, the Gibbs free energy of the system

would increase, assuming the change of enthalpy due to the interpenetration of two polymer layers is negligible, i.e., $\Delta H \approx 0$, according to:

$$\Delta G = \Delta H - T\Delta S > 0$$

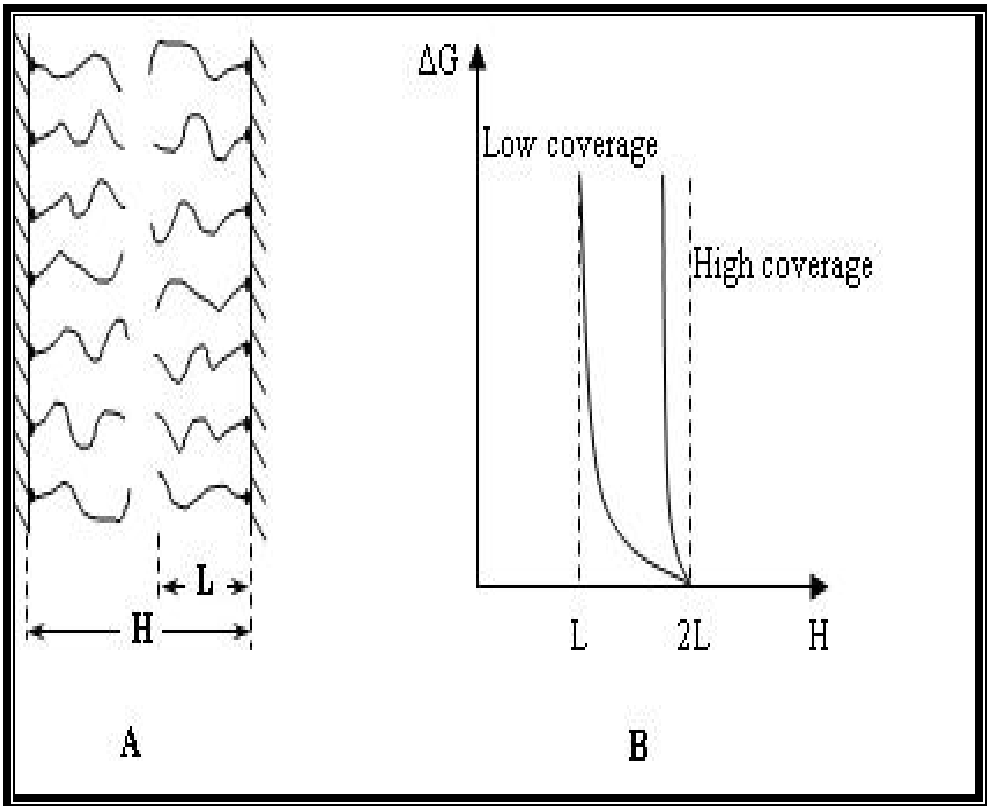

Figure 3.4: A) Interactions between polymer layers covered with anchored polymers B) Sketches the Gibbs free energy as a function of the distance between two particles [17]

So two particles repel one another and the distance between two particles must be equal to or larger than twice the thickness of polymer layers. When the coverage of polymer is high, particularly approaching 100%, there would be no interpenetration. As a result, the two polymer layers will be compressed, leading to the coil up of polymers in both layers. The overall Gibbs free energy increases, and repels the two particles apart. When the

distance between the surfaces of two particles is less than the thickness of polymer layers, a further reduction of the distance would force polymers to coil up and result in an increase in the Gibbs' free energy. Figure 3.4 B sketches the Gibbs free energy as a function of the distance between two particles, and shows that the overall energy is always positive and increases with a decreasing distance when H is smaller than 2L.

The situation is rather different in a poor solvent, with a low coverage of polymer on the solid surface. With a low coverage, when the distance between two particles is less than twice the thickness of polymer layers but larger than the thickness of single polymer layer, i.e., $L < H < 2L$, the polymers adsorbed onto the surface of one particle surface tend to penetrate into the polymer layer of the approach particle. Such interpenetration of two polymer layers will promote further coil up of the polymers, and result in a reduction of the overall Gibbs free energy. Two particles tend to associate with one another. However, with a high coverage, similar to the polymer in a good solvent, there would be no penetration and the reduction in distance results in a compressive force, leading to an increase in the overall free energy. When the distance between two particles is less than the thickness of the polymer layer, a reduction in distance always produces a repulsive force and an increase in the overall Gibbs free energy. Figure 3.5 summarizes the dependence of free energy as a function of distance between two particles.

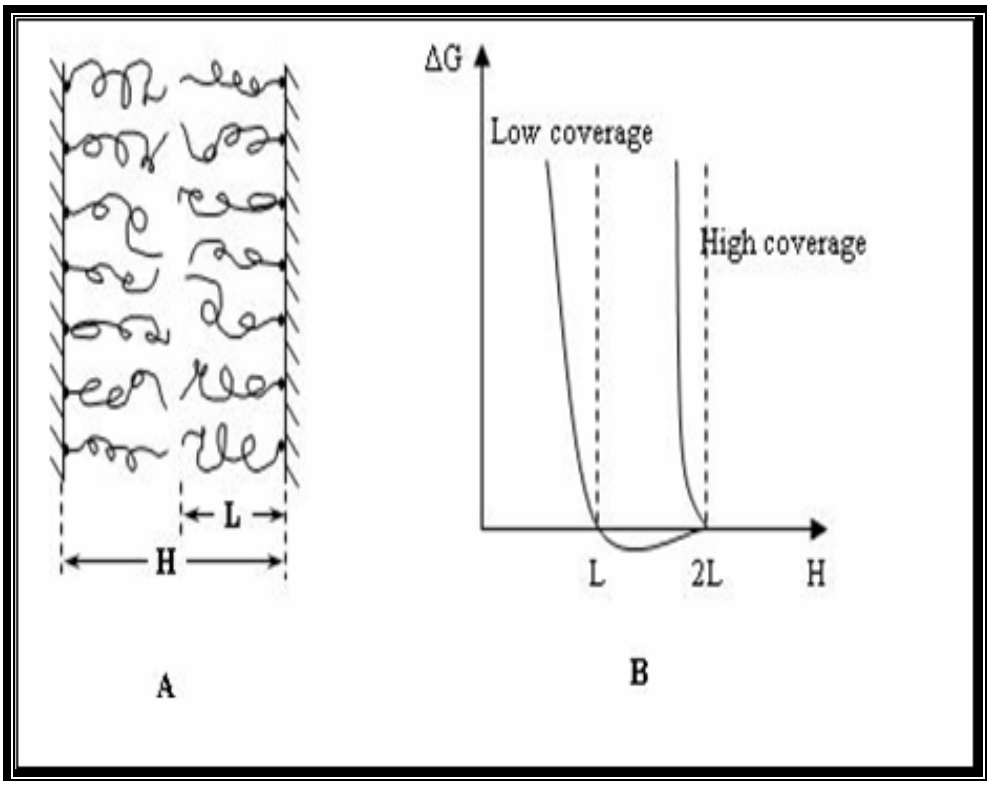

Figure 3.5: Dependence of free energy as a function of distance between two particles [17]

Regardless of the difference in coverage and solvent, two particles covered with polymer layers are prevented from agglomeration by the space exclusion or steric stabilization.

Next, let us look at the adsorbing polymers. The situation of adsorbing polymers is more complicated due to the following two reasons. First, polymer originally attached to the solid surface of one particle may interact with and adsorb onto the other particle surface, and thus form bridges between two particles, when two particles approach to a sufficiently close distance between each other. Second, given sufficient time, attached polymer desorbs from the surface and migrates out of the polymer layer.

When the polymer has a strong adsorption and forms a full coverage, interaction between two polymer layers produces a purely repulsive force and results in increased free energy, when the distance between two particles reduces below twice the thickness of polymer layer. This is the same as that of anchored polymer at full coverage. When only a partial coverage is achieved, the nature of solvent can have a significant influence on the interaction between two particles. In a good solvent, two partially covered polymer layers interpenetrate into each other, resulting in a reduced space and more ordered polymer arrangement. As a result, the entropy reduces and the Gibbs free energy increases. However, in a poor solvent, interpenetration promotes further coil up of polymers, leads to increased entropy, and thus results in a reduced free energy. Invariably a repulsive force develops and repels two particles away from each other, when the distance is less than the thickness of polymer layer [17, 34, 35].

The physical basis for the steric stabilization is: (1) a volume restriction effect arises from the decrease in possible configurations in the region between the two surfaces when two particles approach one another, and (2) an osmotic effect due to the relatively high concentration of adsorbed polymeric molecules in the region between the two particles.

3.4. Results and discussion

An FTIR spectrum of as-received AAMCAB polymer is shown in figure 3.6. The absorption peaks of 2966, 2877, 1754, 1368, 1235, 1174, 1048, 921, and 602 cm^{-1} were observed. The bond assignments for this spectrum are given in table 3.2.

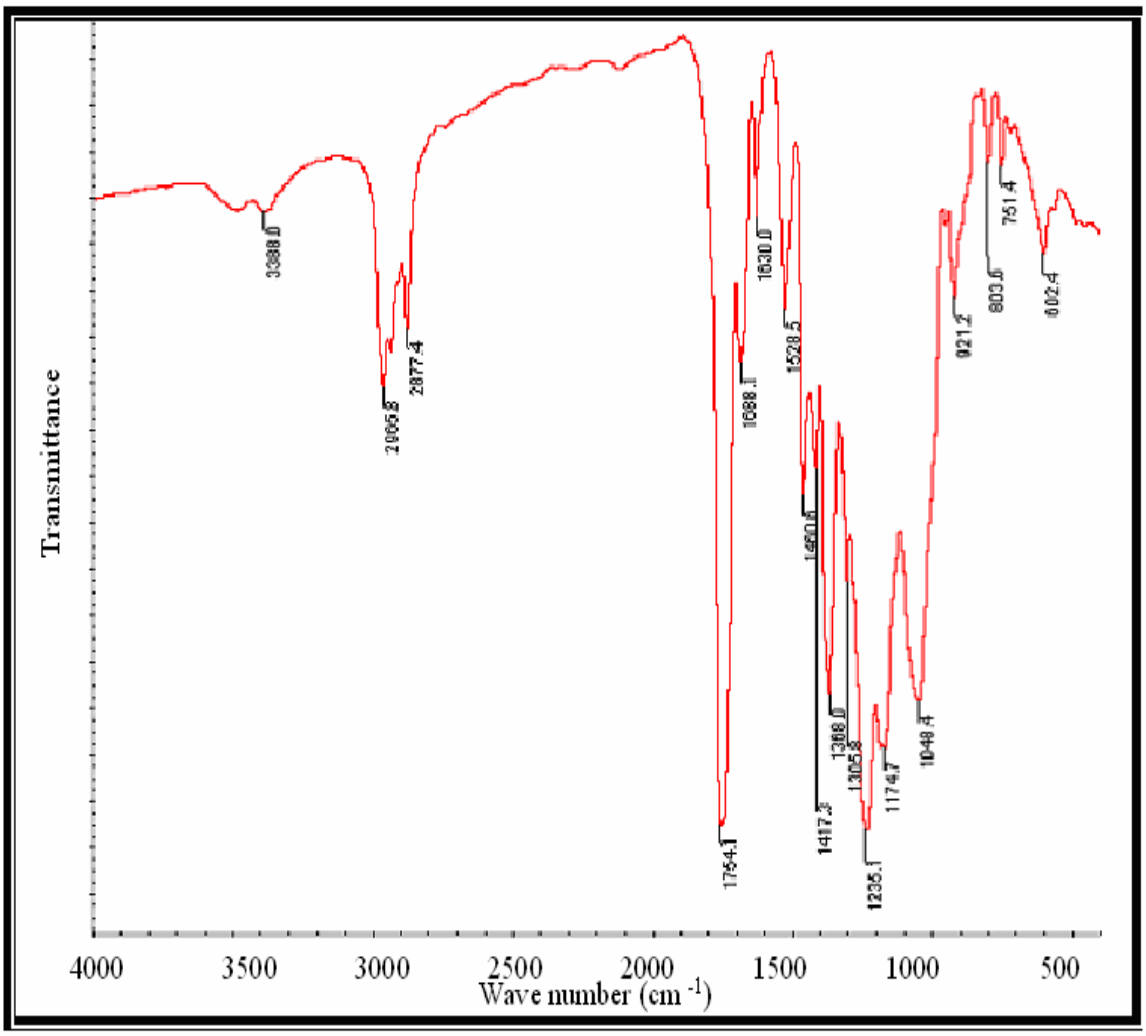

Figure 3.6: FTIR spectrum of AAMCAB polymer

Peaks	Wave number, cm^{-1}	Assignments
1	2966	CH_3 asymmetric stretching
2	2877	CH_3 asymmetric stretching
3	1754	C=O stretching
4	1368	CH symmetric bending
5	1235	C-O stretching
6	1174	Symmetric C-O-C stretch
7	921	Ring symmetric stretching
8	602	OH out of plane bending

Table 3.2: Characteristics bond assignment of AAMCAB polymer

The FTIR spectra of Fe_2O_3 infiltrated with AAMCAB is shown in figure 3.7. The absorption peaks of 1753, 1529, 1460, 1418, 1367, 1306, 1233, 1172, 1050, 635 and 582 cm^{-1} were observed. The bond assignments for this spectrum are given in table 3.3.

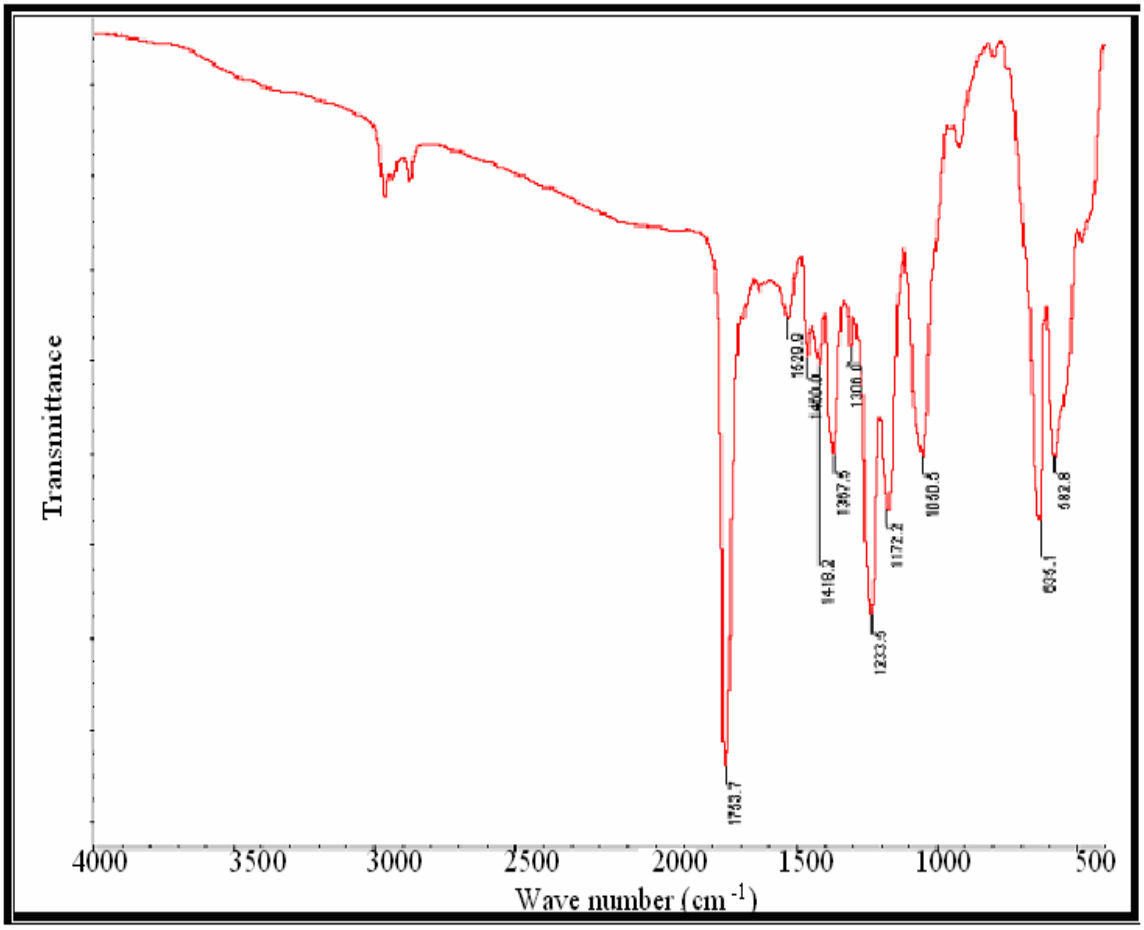

Figure 3.7: FTIR spectrum of Fe_2O_3 gel modified with AAMCAB polymer

Peaks	Wave number, cm^{-1}	Assignments
1	1753	C=O strong stretch
2	1529	N-H bending
3	1460	C-H bending
4	1418	C-H bending
5	1367	C-H scissoring and bending
6	1306	C-N stretch
7	1233	C-N stretch
8	1172	C-N stretch
9	1050	C-O stretch
10	635	C-H bend
11	582	FeO

Table 3.3: Characteristic bond assignment of Fe_2O_3 gel modified with AAMCAB polymer

The CTBN binder was characterized for DSC and TGA. As can be seen from the profile in figure 3.8, this Acrylonitrile binder releases energy above 225ºC, which will be useful to maintain hot spot energy density between fuel and oxidizer.

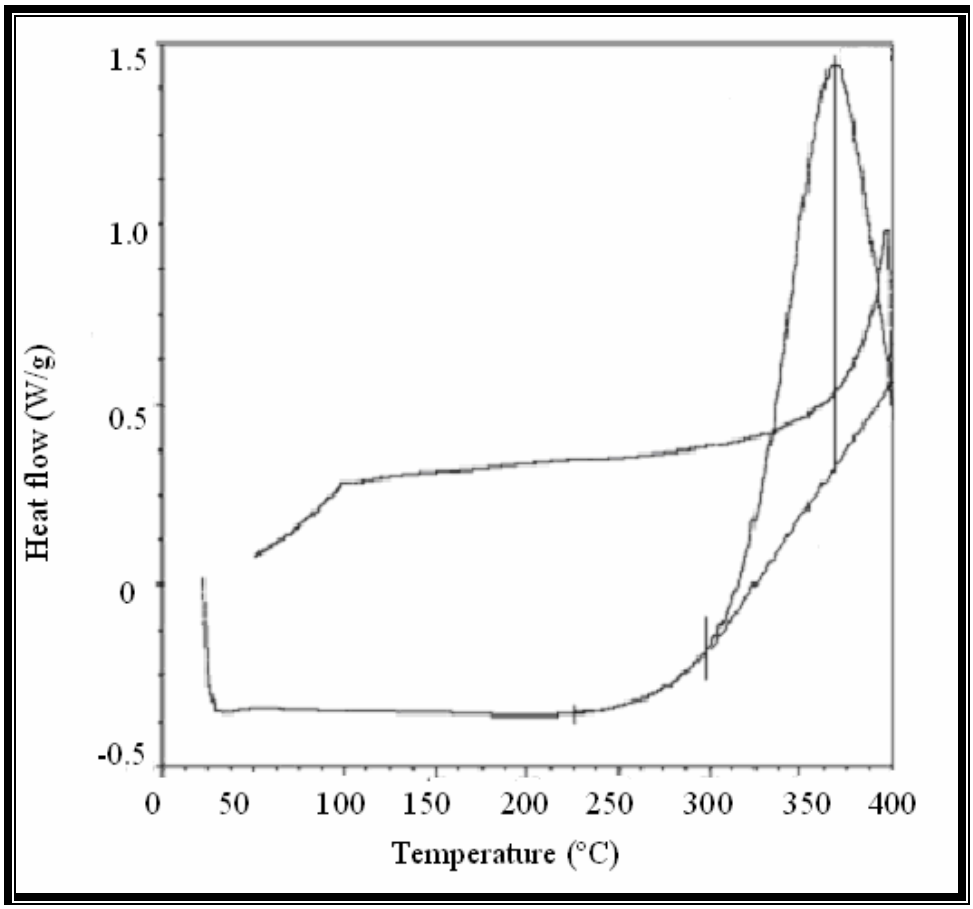

Figure 3.8: DSC profile of acrylonitrile binder

Also the TGA profile in figure 3.9 suggests that the rate of degradation of this kind of binder is slower which will be useful for propellant characteristics.

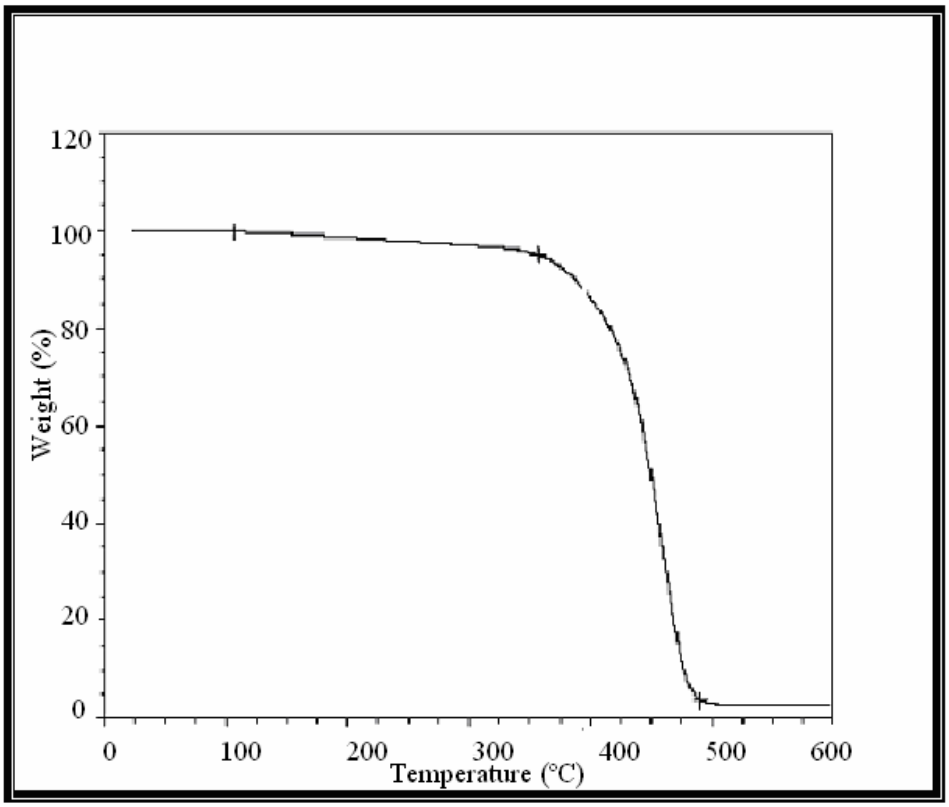

Figure 3.9: TGA profile of PVB and Acrylonitrile binders

CHAPTER 4

BURN RATE AND PRESSURE MEASUREMENTS

4.1 Introduction:

The burn rates of energetic composites are measured as a function of oxidizer and fuel composition [18, 30]. The oxidizers considered are not only Fe_2O_3 particles and gels but, also different gels impregnated with polymers. Al-nanoparticles, CTBN coated Al particles, and CTBN coated and separated were used to prepare the energetic composite. The burn rates were measured by optical sensing method as well as on-chip method [19]. The peak pressure and profiles were measured, for the gels modified with and without the infiltrating the polymer.

Aluminum particles are pyrophoric and are therefore coated with an Al_2O_3 passivation shell. All Al particles contain this shell of about 2 nm size. The surface area-to-volume ratio becomes increasingly large when particle size is reduced to the nanoscale and the total amount of Al_2O_3 accordingly increases. As the size of particles varies, the active aluminum content also changes. Therefore, for preparing the energetic composite, the amount of Al-nanoparticles used was based on the equivalence ratio, which is defined as follows

$$\Phi = \frac{(F/A)actual}{(F/A)stoichiometric}$$

Where, A is the oxidizer and F is the fuel [2, 18, 30].

The oxidizers and Al-nanoparticles were mixed using sonication methods. The sonication process helps to break the particle agglomerates and ensures homogenous mixing of the fuel and oxidizers.

4.2 Experimental

4.2.1 Thermite preparation: Accurately weighed 0.2 g of oxidizer was mixed with 0.094 g of Al-nanoparticles in 2-propanol and sonicated in ultrasonic bath for 6-8 hrs. After sonication, the mixture was transferred on an open pan and dried at about 90-95^{o}C for 10-15 min.

4.2.2 Burn rate measurement set-up:

There are two ways of characterizing the burn rate. One is the open wave velocity propagation and the other is the confined burn flame propagation speed. The open burn characterization is done by initiating the composite in an open environment and measuring the speed at which the flames propagate in the material. In this method the composite material is open to the atmospheric heat loss and also is prone to interaction with atmospheric gases.

The other way is confined wave velocity characterization. In this method the material is initiated in a confined environment and the wave velocity is measured. The confined burn rates for the thermite based energetic is higher than the open burn rate, the reason being that there is less heat loss to the atmosphere hence more amount of heat produced goes into initiating the composite material further and due to absence of atmospheric oxygen

the possibility of the molten aluminum getting oxidized into alumina without taking part in the thermite reaction process is eliminated. Although the reactants and products are solids, gaseous intermediates may be generated during the reaction and condense into solids after flame propagation. It is possible that gaseous intermediates will exist with these high flame temperatures. The build-up of gaseous intermediates will increase the pressure in the confined tube and aid in propelling the flamefront forward. Pressure build up may also result from the high temperate expansion of the air within the pores of the powder mixture. Both theories support the observations that the bulk movement of gas and particulates is integral in determining burn rates. This behavior is consistent with convective burning. A confined set-up for both, the wave velocity measurement and the pressure measurement are as shown below.

4.2.2.1 Optical method: The set-up to test the burn rate is shown in the figure. 4.1. An aluminum block of 10 cm in length was machined to place a Lexane tube containing energetic materials. The block was mounted with four optical sensors, which were connected to photodiodes and this in turn is connected to the oscilloscope.

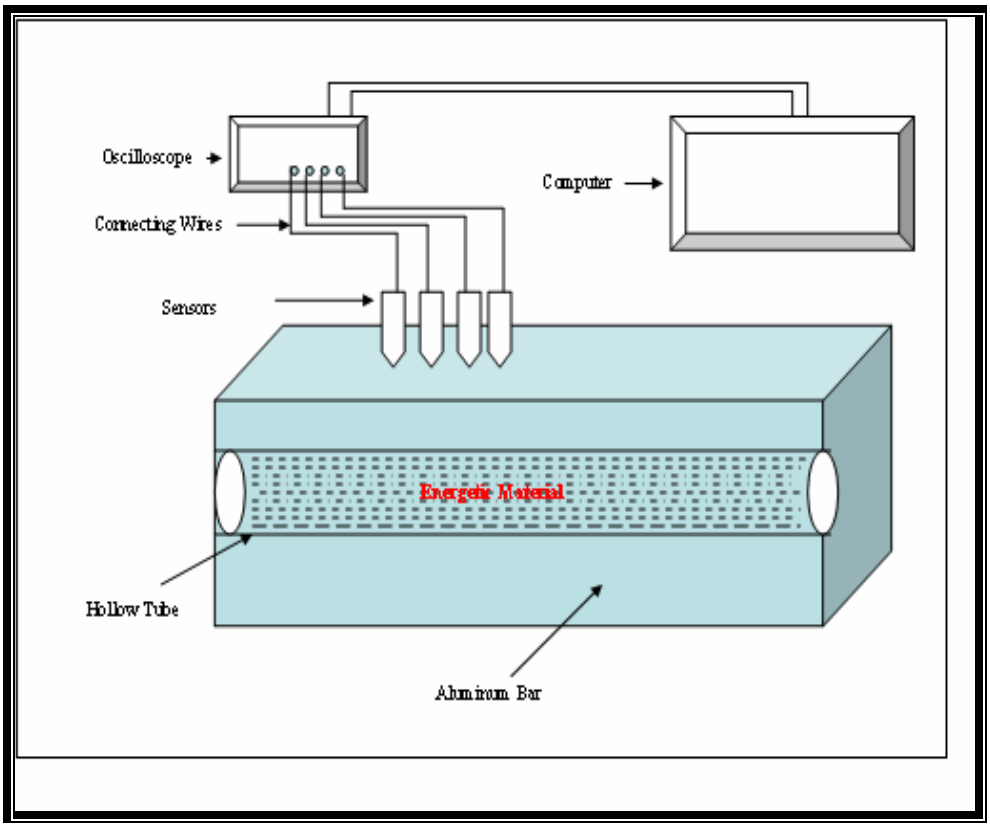

Figure 4.1: Burn rate apparatus setup

The entire set-up was placed inside a metal enclosure; the exhaust of this enclosure was connected to the vacuum exhaust.

4.2.2.2Pressure measurement: The set-up to test the pressure measurement is shown in the figure. 4.2. Aluminum block was designed and machined to hold a Lexane tube containing energetic materials. Two pressure sensors (PCB model A11303A) were mounted on this block and connected to the oscilloscope via a signal conditioner. The measurement of all readings will be preformed in a confined set-up as shown.

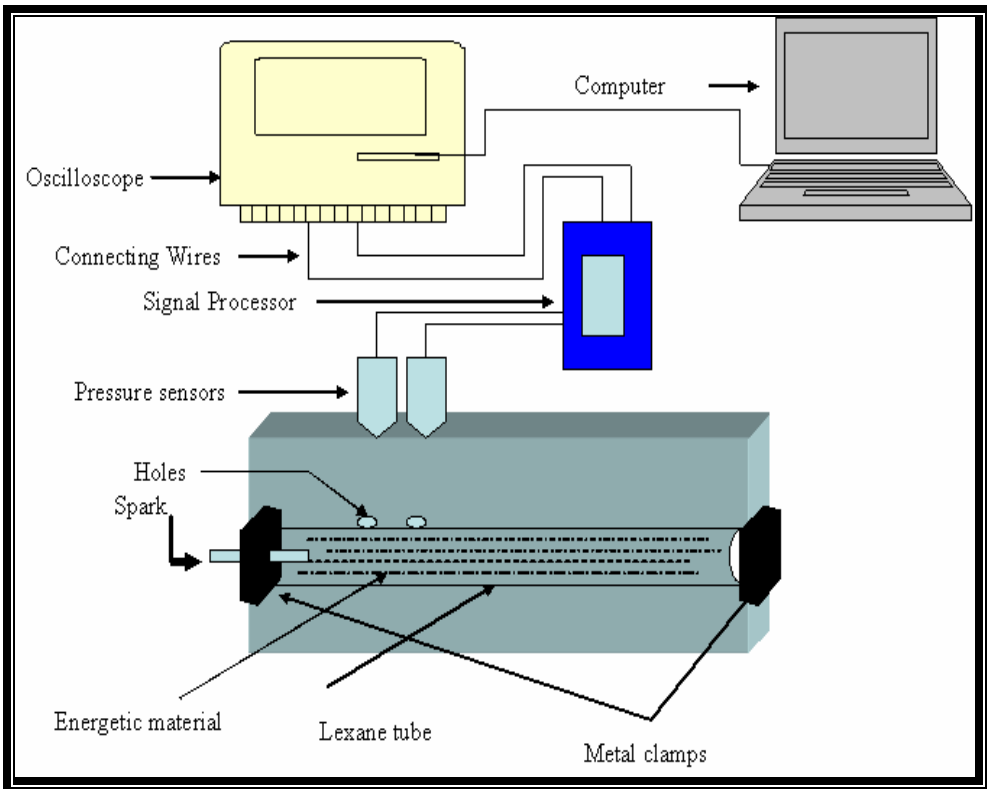

Figure 4.2: Schematic of pressure measurement

4.3 Results and Discussion

For traditional thermite mixtures composed of micron-scale fuel and oxidizer particles, fuel-rich composites, typically produce the highest burn rates. This behavior may result from the increasing thermal conductivity of the composition with increasing metal percentage. For micron-scale particle composites diffusive mechanisms are dominant in flame propagation and a high mixture thermal conductivity will enhance heat transfer and may lead to high burn rates. This behavior will be limited by the amount of oxidizer available in the mixture. Fuel rich mixtures simply have less oxidizer available to optimize burning behavior. Therefore, the fuel and oxidizers were mixed at an optimized

equivalence ratio of 1.4 [13]. The weight of oxidizer and Al-nanoparticles taken are given in table 4.1.

Optimized Φ	Fe_2O_3 (mg)	Al (mg)
1.4	200	94
1.4	400	188
1.4	500	236

Table 4.1: Weights of optimized Fe_2O_3 & Al

Prepared gels can adsorb water very easily, and if this gel is combined with Al-nanoparticles, the rate and the extent of energy release can be reduced. Therefore, for burn rate measurements, the gel samples were heated to 400ºC prior to mixing with Al-nanoparticles.

Nanoenergetic composites	Average Burn Rate (m/s)
Fe_2O_3 gel + Al (80nm)	365
Fe_2O_3 gel + Al (115nm)	94.5
Fe_2O_3sol-gel + 5%AAMCAB+ Al (120 nm) 10% CTBN Coated	38.5

Table 4.2: Burn rate of various nanoenergetic composites

The burn rate of Fe_2O_3 particles and Fe_2O_3 porous gel mixed with Al (80 nm) was 575 m/s, and 365 m/s, respectively. The burn rate value was decreased to 94.5 m/s when 115 nm sized Al-nanoparticles were mixed with porous Fe_2O_3 gel. The combustion wave

velocity values are summarized in table 4.2 and shown as a bar plot in figure 4.3 (next page). This figure shows that as Al-particle size increases, the burn rate decreases. Also, as polymer modified oxidizer and fuel are combined, the burn rate further decreases.

The gel was loaded with 5%AAMCAB polymer as per the procedure outlined in chapter 3. This polymer modified porous gel was mixed with Al-nanoparticles (120 nm) previously coated with 10% CTBN polymeric binder. The combustion velocity of this composite was decreased further to about 38 m/s. These results that are presented in table 4.2 indicate that the combustion wave velocity reduces when particle size increased and Al-nanoparticles coated with CTBN and polymer infiltrated Fe_2O_3 gels were used. The confined burns show an increase in burn rates over the unconfined burns.

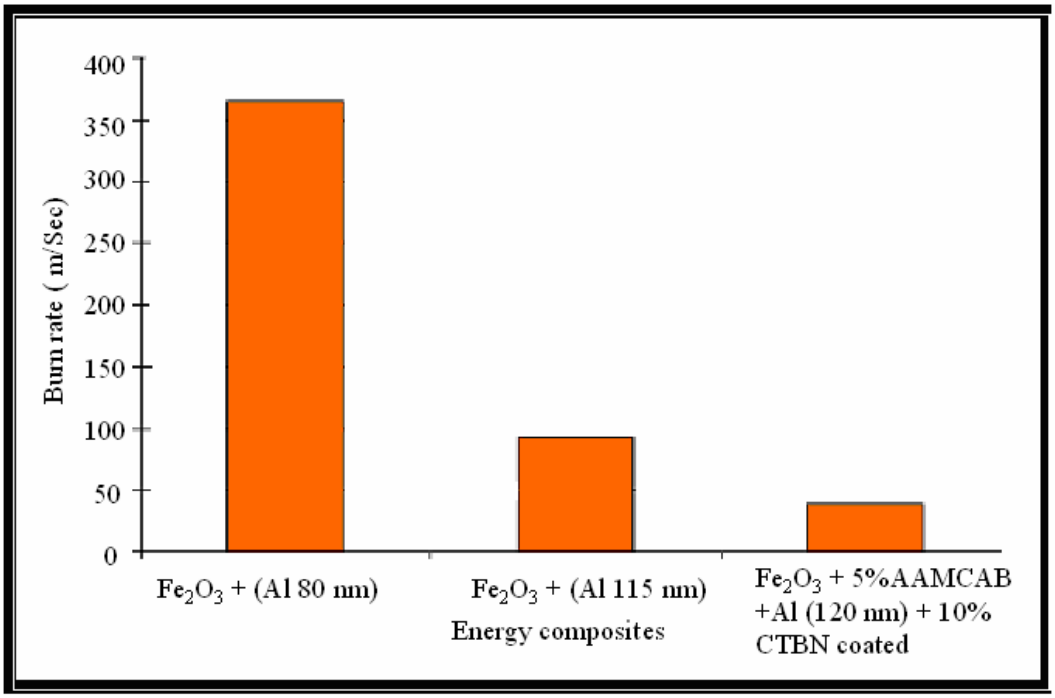

Figure 4.3: Combustion wave velocity of various Fe_2O_3 gel based energetic composites

The pressure as a function of time was measured in confined arrangement for the Fe_2O_3 gel loaded with 2.5% AAMCAB polymer and mixed with Al (80 nm) particles. A plot of pressure vs. time is shown in figure 4.4 for 100 mg of material used in a Lexane tube of 0.8 cc. The pressure increases up to 3.25 and decreases over a period of time.

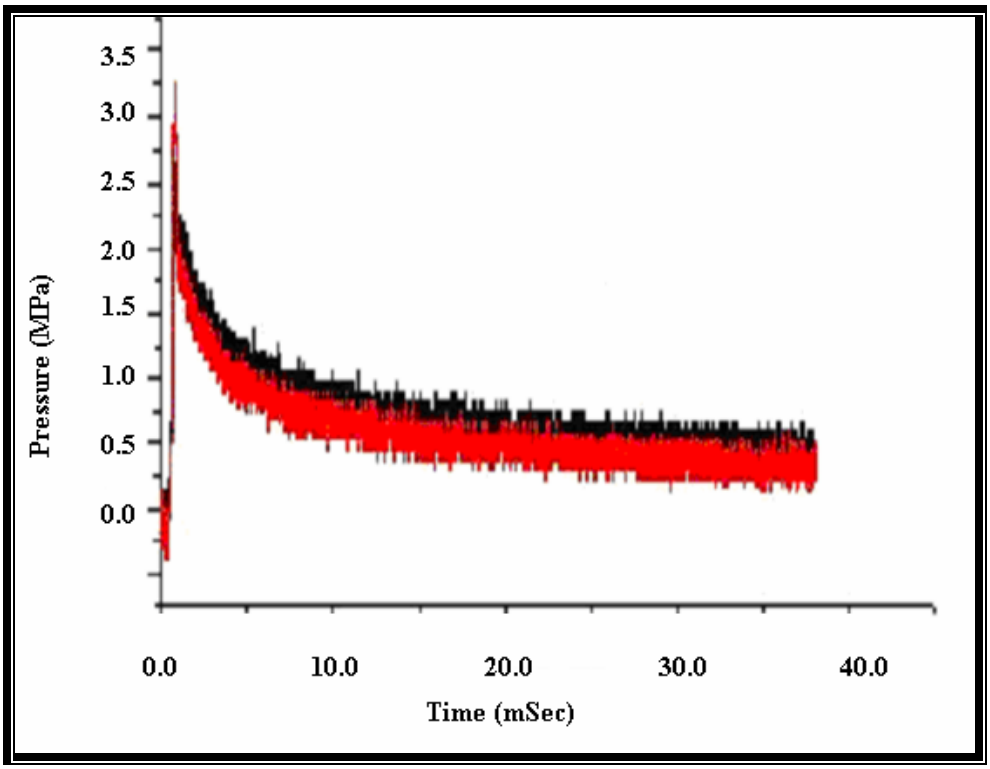

Figure 4.4: Pressure vs. time for Fe_2O_3 gel loaded with 2.5% AAMCAB and mixed with 80 nm Al-nanoparticles, total mass taken 100 mg

Figure 4.5 shows peak pressure and profile for 400 mg of for Fe_2O_3 gel loaded with 2.5% AAMCAB and mixed with 80 nm Al-nanoparticle used. At this material mass, a six fold increase in pressure was observed.

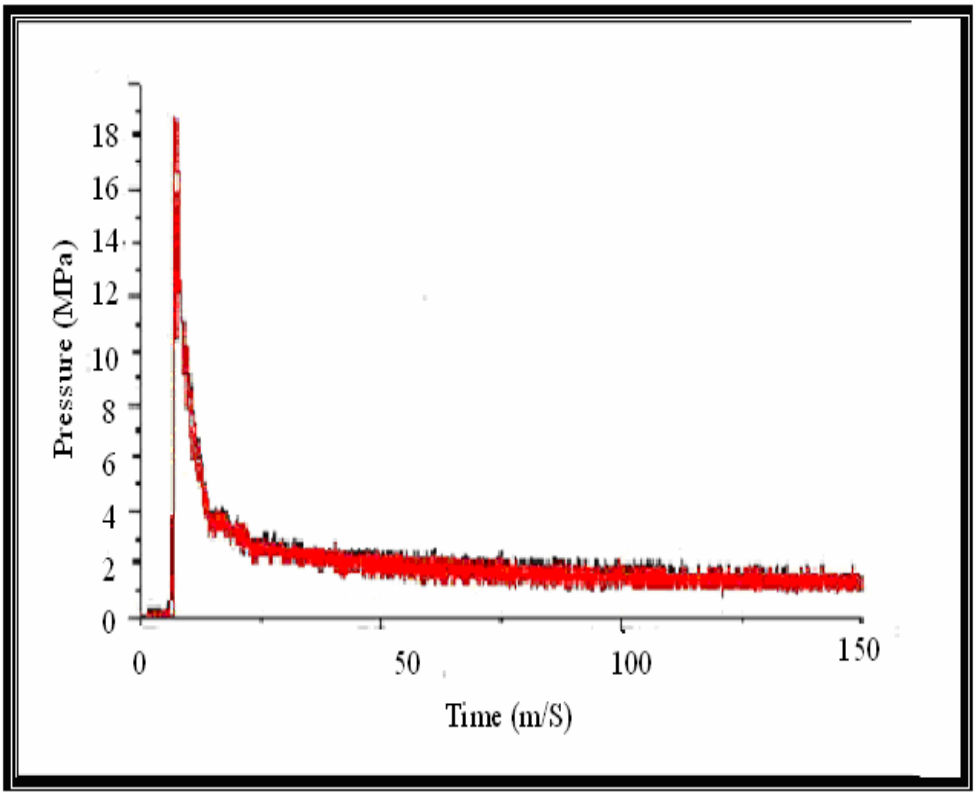

Figure 4.5: Pressure vs. time for Fe_2O_3 gel loaded with 2.5% AAMCAB and mixed with 80 nm Al-nanoparticles, total mass taken 400 mg

Percent theoretical maximum density (%TMD) was varied by changing the sample weight in a fixed volume of 0.8 cc of Lexane tube. Four such %TMD values were chosen and peak pressure and burn rates were measured for the composite of Fe_2O_3 infiltrated with 2.5% AAMCAB polymer mixed with 80 nm. The results are tabulated in table 4.3.

Sample	Peak Pressure, MPa	Burn rate, m/s
100	3.25	152
200	7.55	175
300	13.6	190
400	18.5	200

Table 4.3: Burn rates and pressure for Fe_2O_3 sol-gel + 2.5% AAMCAB + Al (80 nm)

The values of peak pressure and burn rate obtained at various theoretical maximum density %TMD values have been correlated. The burn rate as a function of pressure is shown in figure 4.6, which gives a relationship of $r = 127 \times p^{0.157}$ where r is the burn rate and p is the peak pressure. This relationship will be useful to determine burn rate or peak pressure at other %TMD values [5].

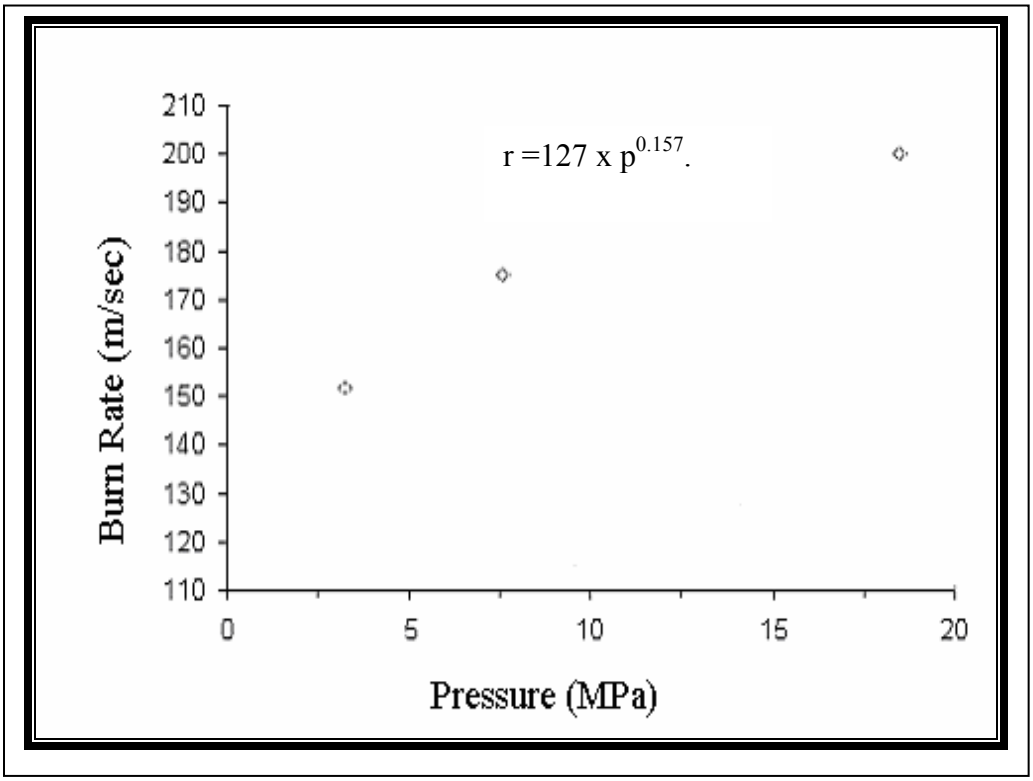

Figure 4.6: Pressure measurement of Fe_2O_3 sol-gel+ 2.5% AAMCAB + Al (80 nm)

In another set of experiments, Fe_2O_3 gel was loaded with 5% AAMCAB and mixed with 10%CTBN coated Al (120 nm) particles. About 50 mg of this composite was ignited in a closed confinement to obtain pressure profile. The pressure vs. time plot is shown in figure 4.7, which indicates that the pressure increased up to about 0.35 MPa and

decreased over a period of 15 ms..It is possible that 50 mg sample has lower %TMD value, which did not reflect in sustained pressure characteristics.

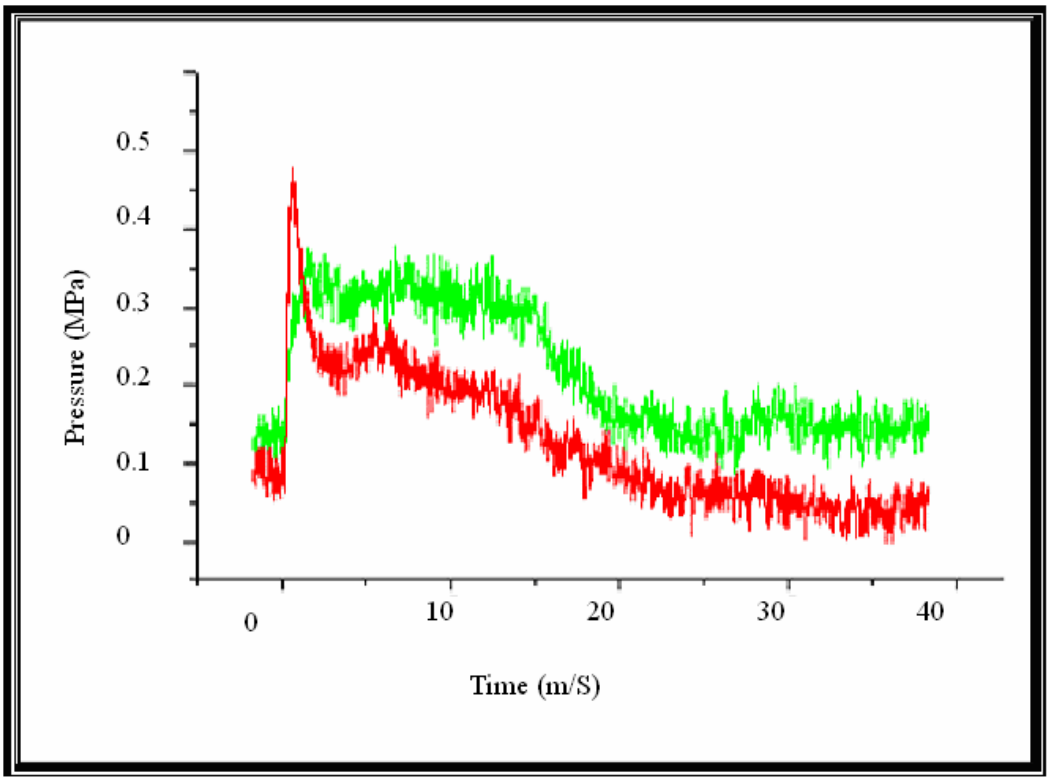

Figure 4.7: Pressure vs. time for Fe_2O_3 Sol-gel+5%AAMCAB+ 10% CTBN coated Al (120 nm) nanoparticles

The pressure characteristics of the composite are shown in figure. 4.8 was prepared with 10%CTBN coated and phase separated Al-nanoparticles. The peak pressure of 2.3 MPa was obtained from 150 mg of sample, which gradually decreased and sustained over a period of 40 ms.

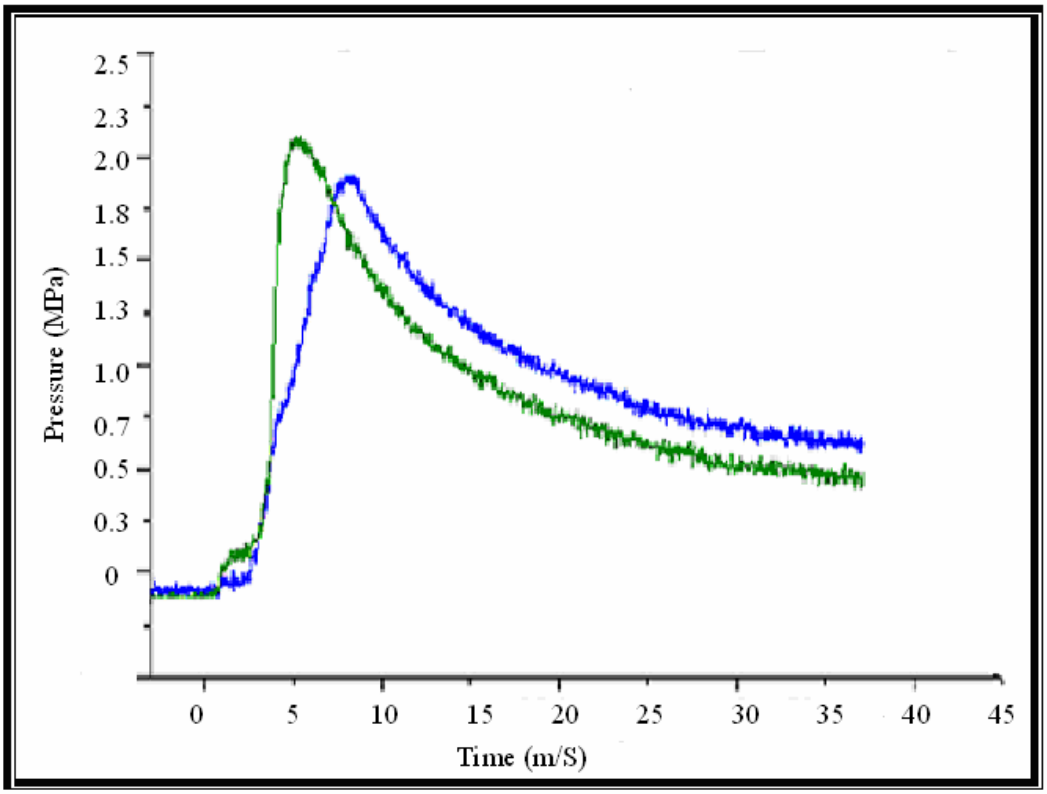

Figure 4.8: Pressure measurement of Fe_2O_3 Sol-gel+5%AAMCAB+ Al (120 nm) 10% CTBN coated phase separated

From the burn rate and pressure data obtained for various porous Fe_2O_3 based energetic composites, it suggests that the composite containing porous gel modified with 5%AAMCAB polymer and combined with 10% CTBN coated and phase separated Al-nanoparticles will be useful for propellant applications as it has slower burn rate and sustained pressure profiles. This response can further be improved if higher percentage of polymer is infiltrated inside porous Fe_2O_3 gels.

CHAPTER 5

ELECTRO STATIC DISCHARGE SENSITIVITY

5.1 Introduction:

Static charges are generally created when dissimilar objects are brought into contact with each other and then separated. When this situation occurs, electrons are transferred from one object to the other. If these objects are electrostatically conductive and both are connected to a third conductive body or to each other, the built up static charge will flow from one body to the other in a short time. The resulting net charge build-up will be zero. If on the other hand, these same electrostatically charged objects are separated by an insulator the charge build-up may not be neutralized and each body may retain its charge for a long time, particularly in a low humidity environment.

Most static electricity is generated by tribocharging, which occurs when two materials come in contact with each other and then are separated [20]. If an atom loses an electron, it becomes positively charged and negatively charged if it gains an electron as shown in figure. 5.1A. Charges (electrons) are exchanged by the materials, leaving one material positively charged and other material negatively charged as shown in figure. 5.1B.

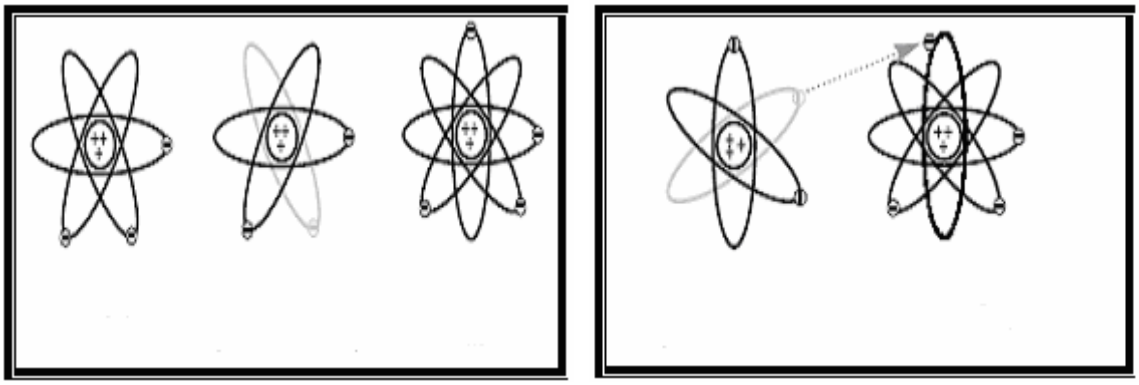

Figure 5.1: A) Exchange of electrons, B) Tribocharging – charge transfer [20]

The charging of objects due to relative motion is known as the triboelectric effect and can produce voltages from a few volts to tens of thousand of volts. The charge build-up depends on many factors including the amount and rate of motion, the composition of the materials involved, the secondary surfaces involved (floor, table top, air, etc,). When the relative humidity level of the air surrounding the charged body is brought near an electrostatically neutral body or one that has an opposite charge, a rapid discharge can occur [3, 20]. In many cases, this discharge is nothing more than an annoyance, however, it could contain sufficient energy to ignite an explosive product or mixture or activate a device initiator used in automotive, defense and space applications [3, 27].

In energetic materials and other energetic formulations, aluminum (Al) - nanoparticles are added to improve performance. For instance addition of Al in propellants is known to increase burn rate [21, 36]. However study shows that the Al particles sensitize explosive formulation to ESD [22, 23]. This study further reveals that that for Al particle size of 20-90 nm the ESD ignition energy is .0006 J, whereas for particle size of 180 nm, the energy increased to > 0.156 J. This suggests that the ignition energy required for bigger particles

is higher than for the smaller particles, however bigger particles have lower surface area and less reactivity, which can prevent improvement in performance of energetic material. Smaller Al particles have much higher sensitivity to ESD possibly making MIC more sensitive to ESD. MIC materials have very high burn rates; however their ESD sensitivity is a critical issue.

Few attempts have been reported in the literature to reduce the sensitivity of Al particles. In one research effort, Al-nanoparticles (20-50 nm) were coated with fluoropolymer (Teflon) at 18% mass percent level. Originally these particles had ESD ignition energy of 0.006 J. On coating with fluoropolymer, their ESD energy value was increased to >0.156 J [22, 23]. However, the fluropolymer coated Al-nanoparticles enhanced impact sensitivity of explosives. Another polymer, glyciadal azide polymer (GAP), when mixed with Al-nanoparticles in a ratio of 50:50 did not show sensitivity towards ESD, impact and friction [22, 23]. Several other polymers are also used to improve ESD ignition sensitivity to ESD ignition. It was also noted that coating of ultra fine Al particles with aluminum carbide to reduce reactivity towards water and oxygen, which may reduce sensitivity to ESD ignition [24].

We used CTBN polymeric binder to coat Al-nanoparticles to reduce ESD ignition sensitivity energy of energetic composites.

5.2 Experimental:

5.2.1 Al-nanoparticles: Al-nanoparticles of 50-120 nm were obtained from Nanotechnologies Inc., TX and used as-received for ESD ignition energy measurements.

5.2.2 CTBN coated Al-nanoparticles: To 100 ml of 2-butanone 10 gms of CTBN polymer was added. This solution was gently heated to dissolve the polymer. When the polymer was completely dissolved a light yellow colored solution was formed. To this solution a drop of K-sperse 152 (zinc alkylaryl sulfonate ethylene glycol mono butyl ether), a dispersant was added. A measured quantity of nanoaluminum powder was added to it to achieve 2.5% and 5% (w/v) of CTBN loadings. The mixture was sonicated for 24-48 hrs to ensure dispersion of most of the Al- particles. This was heated on an open pan at about 80ºC to evaporate the solvent.

5.2.3 Nanoenergetic composite: Accurately weighed 0.2 g of oxidizer was mixed with 0.094 g of Al-nanoparticles in 2-propanol and sonicated in ultrasonic bath for 6-8 hrs. After sonication, the mixture was transferred to an open pan and dried at about 90-95^{o}C for 10-15 min.

5.2.4 ESD ignition energy measurement: The Model 931 test system from Safety Management Services, Utah, was used to measure the ESD energy of ignition. A small quantity (approx.10 mg) is placed in the plastic washer (0.3 mm diameter) which was filled with energetic material and placed underneath the discharge needle. The sample was brought closer to the needle so it was touching to the sample. The system was

charged to specific voltages and discharge through the capacitor circuit. This discharge causes the charge dumped onto the sample. The schematic of ESD measurement set-up is shown in figure 5.2.

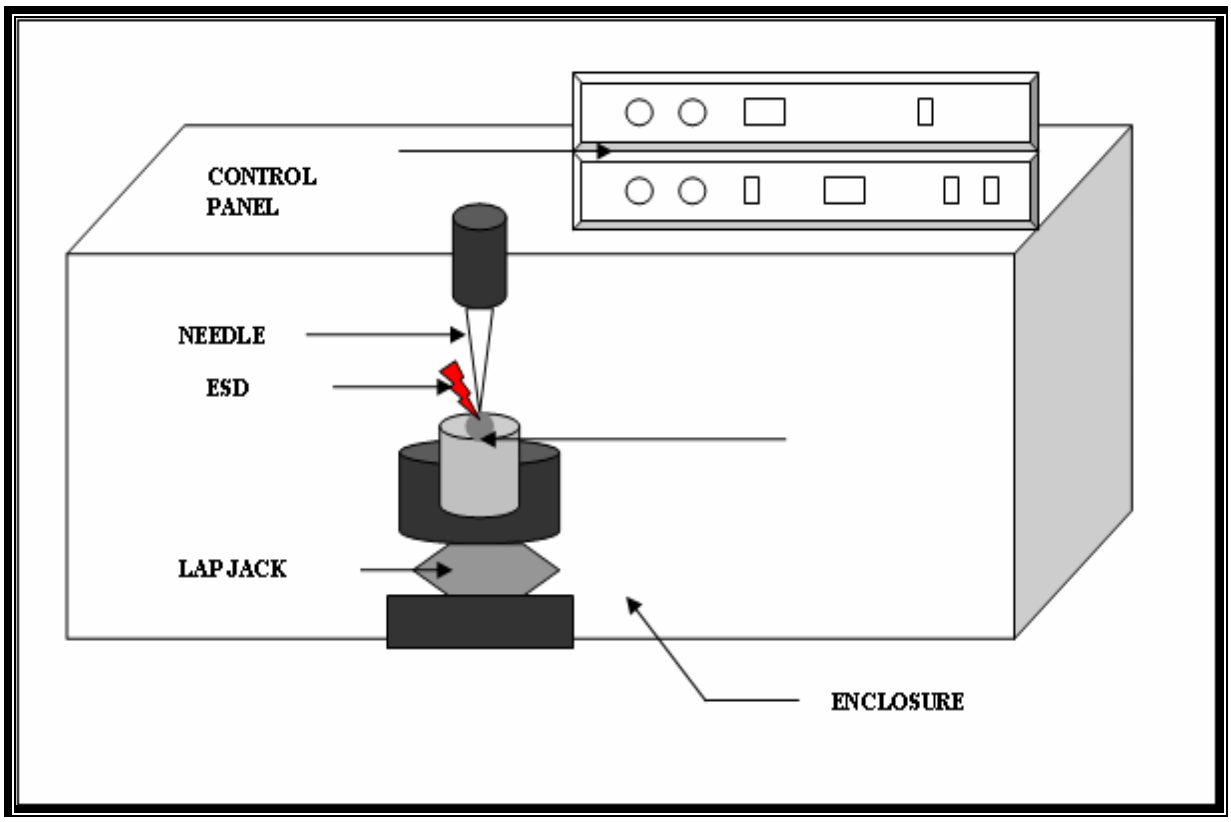

Figure 5.2: ESD set-up

5.3 Results and discussion

The ESD ignition energy of Al-nanoparticles and different formulations of energetic composites were measured. Also the oxidizer and fuel Al which were modified using the polymer and the binder were also tested for their ignition energies. The tables like the sample table 5.0 shown will be used to note the ESD ignition energies. The differences in

capacitance values in the table indicate the labeled value on the instrument to the exact capacitance value. The ignition energy values will be a function of voltage and the discharged capacitance in the sample. The value of the capacitors is in Pico farads and the voltage has the value in volts. The ESD value is measured in milli joules. The legends provided in the lighter shade indicate that the sample survived the ESD energy and the legends in the darker shade indicate that the sample failed to sustain the ESD energy and ignited. That indicated the minimum ignition energy for that particular sample.

		ESD Energy, mJ						
		Capacitance Value						
		300	450	600	1200	2400	10,000	20,000
		3.13E-10	4.45E-10	5.98E-10	1.30E-09	2.50E-09	1.01E-08	2.00E-08
Voltage Level	500	0.04	0.06	0.07	0.16	0.31	1.26	2.5
	1000	0.16	0.22	0.3	0.65	1.25	5.05	10
	1500	0.35	0.5	0.67	1.46	2.81	11.36	22.5
	2000	0.63	0.89	1.2	2.6	5	20.2	40
	2500	0.98	1.39	1.87	4.06	7.81	31.56	62.5
	3000	1.41	2	2.69	5.85	11.25	45.45	90
	3500	1.92	2.73	3.66	7.96	15.31	61.86	122.5
	4000	2.5	3.56	4.78	10.4	20	80.8	160
	4500	3.17	4.51	6.05	13.16	25.31	102.26	202.5
	5000	3.91	5.56	7.48	16.25	31.25	126.25	250

Table 5.0: Specimen Table

Al (50 nm) ESD Energy, mJ							
	Capacitance Value						
Voltage Level	300	450	600	1200	2400	10,000	20,000
	3.13E-10	4.45E-10	5.98E-10	1.30E-09	2.50E-09	1.01E-08	2.00E-08
500	0.04	0.06	0.07	0.16	0.31	1.26	2.50
1000	0.16	0.22	0.30	0.65	1.25	5.05	10.00
1500	0.35	0.50	0.67	1.46	2.81	11.36	22.50
2000	0.63	0.89	1.20	2.60	5.00	20.20	40.00
2500	0.98	1.39	1.87	4.06	7.81	31.56	62.50
3000	1.41	2.00	2.69	5.85	11.25	45.45	90.00
3500	1.92	2.73	3.66	7.96	15.31	61.86	122.50
4000	2.50	3.56	4.78	10.40	20.00	80.80	160.00
4500	3.17	4.51	6.05	13.16	25.31	102.26	202.50
5000	3.91	5.56	7.48	16.25	31.25	126.25	250.00

*All energies are in mJ

Table 5.1: ESD energy values for 50nm Al particles

Al (80 nm) ESD Energy, mJ							
	Capacitance Value						
Voltage Level	300	450	600	1200	2400	10,000	20,000
	3.13E-10	4.45E-10	5.98E-10	1.30E-09	2.50E-09	1.01E-08	2.00E-08
500	0.04	0.06	0.07	0.16	0.31	1.26	2.50
1000	0.16	0.22	0.30	0.65	1.25	5.05	10.00
1500	0.35	0.50	0.67	1.46	2.81	11.36	22.50
2000	0.63	0.89	1.20	2.60	5.00	20.20	40.00
2500	0.98	1.39	1.87	4.06	7.81	31.56	62.50
3000	1.41	2.00	2.69	5.85	11.25	45.45	90.00
3500	1.92	2.73	3.66	7.96	15.31	61.86	122.50
4000	2.50	3.56	4.78	10.40	20.00	80.80	160.00
4500	3.17	4.51	6.05	13.16	25.31	102.26	202.50
5000	3.91	5.56	7.48	16.25	31.25	126.25	250.00

*All energies are in mJ

Table 5.2: ESD energy values for 80nm Al particles

Al (115 nm) ESD Energy, mJ							
				Capacitance Value			
	300	450	600	1200	2400	10,000	20,000
	3.13E-10	4.45E-10	5.98E-10	1.30E-09	2.50E-09	1.01E-08	2.00E-08
500	0.04	0.06	0.07	0.16	0.31	1.26	2.50
1000	0.16	0.22	0.30	0.65	1.25	5.05	10.00
1500	0.35	0.50	0.67	1.46	2.81	11.36	22.50
2000	0.63	0.89	1.20	2.60	5.00	20.20	40.00
2500	0.98	1.39	1.87	4.06	7.81	31.56	62.50
3000	1.41	2.00	2.69	5.85	11.25	45.45	90.00
3500	1.92	2.73	3.66	7.96	15.31	61.86	122.50
4000	2.50	3.56	4.78	10.40	20.00	80.80	160.00
4500	3.17	4.51	6.05	13.16	25.31	102.26	202.50
5000	3.91	5.56	7.48	16.25	31.25	126.25	250.00

Voltage Level

*All energies are in mJ

Table 5.3: ESD energy values for 115 nm Al particles

Al (120 nm) ESD Energy, mJ							
				Capacitance Value			
	300	450	600	1200	2400	10,000	20,000
	3.13E-10	4.45E-10	5.98E-10	1.30E-09	2.50E-09	1.01E-08	2.00E-08
500	0.04	0.06	0.07	0.16	0.31	1.26	2.50
1000	0.16	0.22	0.30	0.65	1.25	5.05	10.00
1500	0.35	0.50	0.67	1.46	2.81	11.36	22.50
2000	0.63	0.89	1.20	2.60	5.00	20.20	40.00
2500	0.98	1.39	1.87	4.06	7.81	31.56	62.50
3000	1.41	2.00	2.69	5.85	11.25	45.45	90.00
3500	1.92	2.73	3.66	7.96	15.31	61.86	122.50
4000	2.50	3.56	4.78	10.40	20.00	80.80	160.00
4500	3.17	4.51	6.05	13.16	25.31	102.26	202.50
5000	3.91	5.56	7.48	16.25	31.25	126.25	250.00

Voltage Level

*All energies are in mJ

Table 5.4: ESD energy values for 120 nm Al particles

From the above tables, it can be observed that for 50 nm particles, the ESD ignition energy is 0.89 mJ whereas for 120 nm particles the energy increases to 3.66 mJ. This shows that with increase in particles size of Al-nanoparticles, ESD ignition energy increases. By CTBN coating, we anticipated that the ESD energy will further increase. The results obtained on ESD ignition energy for 5% and 10% CTBN coated Al-nanoparticles are given in the following tables 5.5, 5.6, 5.7 and 5.8.

Al (115 nm) 10%CTBN coated ESD Energy, mJ

Voltage Level	Capacitance Value						
	300	450	600	1200	2400	10,000	20,000
	3.13E-10	4.45E-10	5.98E-10	1.30E-09	2.50E-09	1.01E-08	2.00E-08
500	0.04	0.06	0.07	0.16	0.31	1.26	2.50
1000	0.16	0.22	0.30	0.65	1.25	5.05	10.00
1500	0.35	0.50	0.67	1.46	2.81	11.36	22.50
2000	0.63	0.89	1.20	2.60	5.00	20.20	40.00
2500	0.98	1.39	1.87	4.06	7.81	31.56	62.50
3000	1.41	2.00	2.69	5.85	11.25	45.45	90.00
3500	1.92	2.73	3.66	7.96	15.31	61.86	122.50
4000	2.50	3.56	4.78	10.40	20.00	80.80	160.00
4500	3.17	4.51	6.05	13.16	25.31	102.26	202.50
5000	3.91	5.56	7.48	16.25	31.25	126.25	250.00

*All energies are in mJ

Table 5.5: ESD energy values for Al (115 nm) particles (10% CTBN Coated)

Al (120 nm) 10% CTBN Coated ESD Energy, mJ

Voltage Level	Capacitance Value						
	300	450	600	1200	2400	10,000	20,000
	3.13E-10	4.45E-10	5.98E-10	1.30E-09	2.50E-09	1.01E-08	2.00E-08
500	0.04	0.06	0.07	0.16	0.31	1.26	2.50
1000	0.16	0.22	0.30	0.65	1.25	5.05	10.00
1500	0.35	0.50	0.67	1.46	2.81	11.36	22.50
2000	0.63	0.89	1.20	2.60	5.00	20.20	40.00
2500	0.98	1.39	1.87	4.06	7.81	31.56	62.50
3000	1.41	2.00	2.69	5.85	11.25	45.45	90.00
3500	1.92	2.73	3.66	7.96	15.31	61.86	122.50
4000	2.50	3.56	4.78	10.40	20.00	80.80	160.00
4500	3.17	4.51	6.05	13.16	25.31	102.26	202.50
5000	3.91	5.56	7.48	16.25	31.25	126.25	250.00

*All energies are in mJ

Table 5.6: ESD energy values for Al (120 nm) 10% CTBN coated

Al (120 nm) 5% CTBN coated ESD Energy, mJ

Voltage Level	Capacitance Value						
	300	450	600	1200	2400	10,000	20,000
	3.13E-10	4.45E-10	5.98E-10	1.30E-09	2.50E-09	1.01E-08	2.00E-08
500	0.04	0.06	0.07	0.16	0.31	1.26	2.50
1000	0.16	0.22	0.30	0.65	1.25	5.05	10.00
1500	0.35	0.50	0.67	1.46	2.81	11.36	22.50
2000	0.63	0.89	1.20	2.60	5.00	20.20	40.00
2500	0.98	1.39	1.87	4.06	7.81	31.56	62.50
3000	1.41	2.00	2.69	5.85	11.25	45.45	90.00
3500	1.92	2.73	3.66	7.96	15.31	61.86	122.50
4000	2.50	3.56	4.78	10.40	20.00	80.80	160.00
4500	3.17	4.51	6.05	13.16	25.31	102.26	202.50
5000	3.91	5.56	7.48	16.25	31.25	126.25	250.00

*All energies are in mJ

Table 5.7 ESD energy values for Al (120 nm) particles 5% CTBN coated

Al (120 nm) 10% CTBN Coated Phase Separated As-in (Phase-Up) ESD Energy, mJ							
		Capacitance Value					
	300	450	600	1200	2400	10,000	20,000
	3.13E-10	4.45E-10	5.98E-10	1.30E-09	2.50E-09	1.01E-08	2.00E-08
Voltage Level 500	0.04	0.06	0.07	0.16	0.31	1.26	2.50
1000	0.16	0.22	0.30	0.65	1.25	5.05	10.00
1500	0.35	0.50	0.67	1.46	2.81	11.36	22.50
2000	0.63	0.89	1.20	2.60	5.00	20.20	40.00
2500	0.98	1.39	1.87	4.06	7.81	31.56	62.50
3000	1.41	2.00	2.69	5.85	11.25	45.45	90.00
3500	1.92	2.73	3.66	7.96	15.31	61.86	122.50
4000	2.50	3.56	4.78	10.40	20.00	80.80	160.00
4500	3.17	4.51	6.05	13.16	25.31	102.26	202.50
5000	3.91	5.56	7.48	16.25	31.25	126.25	250.00
*All energies are in mJ							

Table 5.8: ESD energy values for Al (120 nm) 10% CTBN coated, coated particles separated from the uncoated particles

It is noted that for 120 nm particles coated with 10%CTBN failed at the ESD value of 3.66 mJ. However, when the coated particles were separated from the uncoated ones, the ESD ignition energy is increased significantly to the value of 45.45 mJ. The ESD ignition values are summarized in the figure 5.3 and in table 5.9.

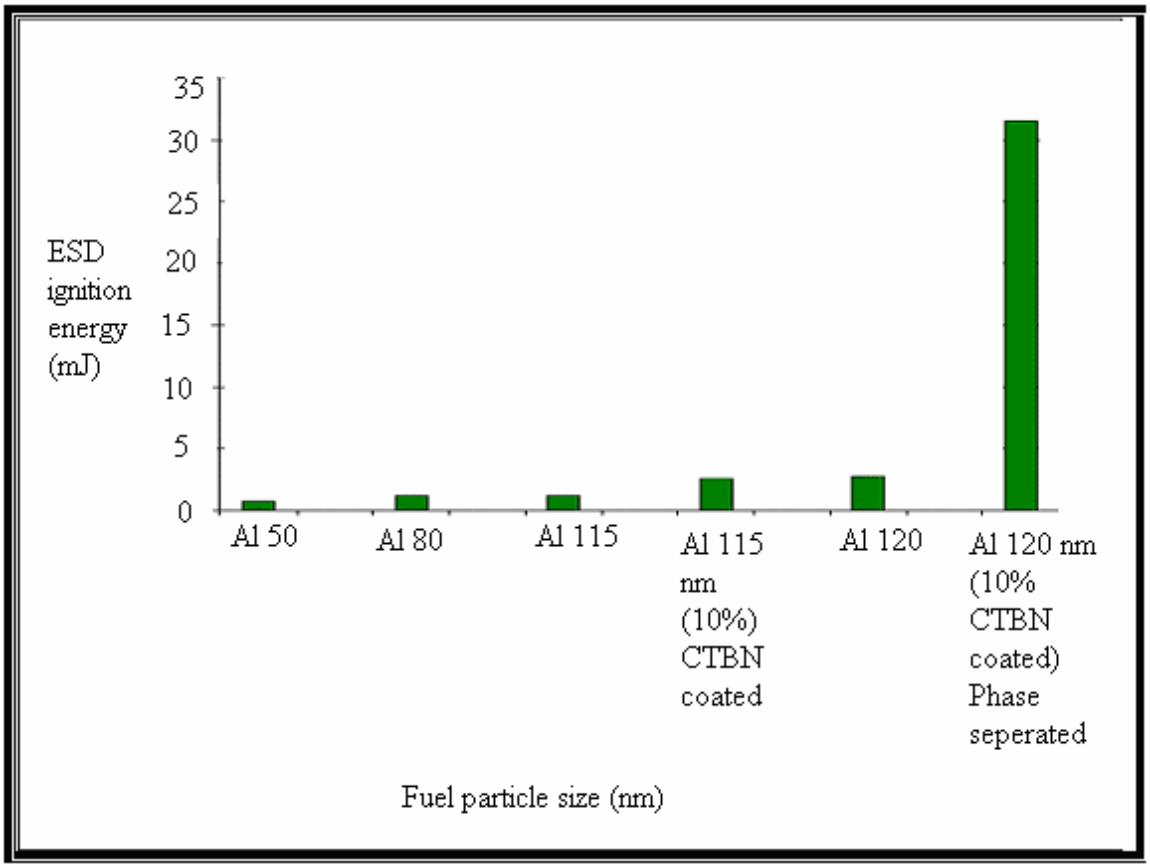

Figure 5.3: Electrostatic Ignition Energy vs. Fuel particle size

Fuel Particle Size (nm)	ESD Ignition Energy(mJ)
Al 50	0.67
Al 80	1.20
Al 115	1.20
Al 115 nm (10% CTBN coated)	2.50
Al 120	2.69
Al 120 nm (10% CTBN coated) phase separated	31.56

Table 5.9: ESD energy of Al-nanoparticles with and without CTBN coating

Fe_2O_3-nanoparticles were mixed Al-nanoparticles (with and without CTBN coating) of different sizes and tested to determine their ESD ignition energy. The tables 5.10 to 5.12 give the values of ESD ignition energy for these energetic composites.

Fe_2O_3 Particles + Al (80 nm) ESD Energy, mJ

Voltage Level	Capacitance Value						
	300	450	600	1200	2400	10,000	20,000
	3.13E-10	4.45E-10	5.98E-10	1.30E-09	2.50E-09	1.01E-08	2.00E-08
500	0.04	0.06	0.07	0.16	0.31	1.26	2.50
1000	0.16	0.22	0.30	0.65	1.25	5.05	10.00
1500	0.35	0.50	0.67	1.46	2.81	11.36	22.50
2000	0.63	0.89	1.20	2.60	5.00	20.20	40.00
2500	0.98	1.39	1.87	4.06	7.81	31.56	62.50
3000	1.41	2.00	2.69	5.85	11.25	45.45	90.00
3500	1.92	2.73	3.66	7.96	15.31	61.86	122.50
4000	**2.50**	3.56	4.78	10.40	20.00	80.80	160.00
4500	3.17	4.51	6.05	13.16	25.31	102.26	202.50
5000	3.91	5.56	7.48	16.25	31.25	126.25	250.00

*All energies are in mJ

Table 5.10: ESD energy values for Fe_2O_3 Particles + Al (80 nm)

Fe_2O_3 Particles + Al (115 nm) ESD Energy, mJ

Voltage Level	Capacitance Value						
	300	450	600	1200	2400	10,000	20,000
	3.13E-10	4.45E-10	5.98E-10	1.30E-09	2.50E-09	1.01E-08	2.00E-08
500	0.04	0.06	0.07	0.16	0.31	1.26	2.50
1000	0.16	0.22	0.30	0.65	1.25	5.05	10.00
1500	0.35	0.50	0.67	1.46	2.81	11.36	22.50
2000	0.63	0.89	1.20	2.60	5.00	20.20	40.00
2500	0.98	1.39	1.87	4.06	7.81	31.56	62.50
3000	1.41	2.00	2.69	5.85	11.25	45.45	90.00
3500	1.92	2.73	3.66	7.96	15.31	61.86	122.50
4000	2.50	3.56	4.78	10.40	20.00	80.80	160.00
4500	3.17	4.51	6.05	13.16	25.31	102.26	202.50
5000	3.91	5.56	7.48	16.25	31.25	126.25	250.00

***All energies are in mJ**

Table 5.11: ESD energy values for Fe_2O_3 Particles + Al (115 nm)

Fe_2O_3 Particles + 1%CTBN COATED Al (80 nm) ESD Energy, mJ

Voltage Level	Capacitance Value						
	300	450	600	1200	2400	10,000	20,000
	3.13E-10	4.45E-10	5.98E-10	1.30E-09	2.50E-09	1.01E-08	2.00E-08
500	0.04	0.06	0.07	0.16	0.31	1.26	2.50
1000	0.16	0.22	0.30	0.65	1.25	5.05	10.00
1500	0.35	0.50	0.67	1.46	2.81	11.36	22.50
2000	0.63	0.89	1.20	2.60	5.00	20.20	40.00
2500	0.98	1.39	1.87	4.06	7.81	31.56	62.50
3000	1.41	2.00	2.69	5.85	11.25	45.45	90.00
3500	1.92	2.73	3.66	7.96	15.31	61.86	122.50
4000	2.50	3.56	4.78	10.40	20.00	80.80	160.00
4500	3.17	4.51	6.05	13.16	25.31	102.26	202.50
5000	3.91	5.56	7.48	16.25	31.25	126.25	250.00

*All energies are in mJ

Table 5.12: ESD energy values for Fe_2O_3 Particles +1% CTBN coated Al (80 nm)

The values indicate that for the composites prepared with Fe_2O_3 Particles mixed with 80 nm with and without CTBN coating (1% w/w) do not differ. However, when 115 nm Al-particles were used, the ESD ignition energy increased to 4.78 mJ. The table 5.13 summarizes ESD ignition values for Fe_2O_3 Particles based energetic composites.

Composite Type (Particles)	**ESD Ignition Energy (mJ)**
Fe_2O_3 Particles + Al (80 nm)	2.50
Fe_2O_3 Particles + Al (115 nm)	4.06
Fe_2O_3 Particles + 2.5% AAMCAB + Al (80 nm)	5.85
Fe_2O_3 Particles + 10% CTBN coated Al (80 nm)	2.50
Fe_2O_3 Particles + 2.5% AAMCAB + CTBN coated Al (80 nm)	5.85
Fe_2O_3 Particles+ 5% AAMCAB+ Al (120 nm) 10% CTBN coated	61.86

Table 5.13: ESD energy values for Fe_2O_3 particles composites

Composites were prepared by mixing porous Fe_2O_3 gels with Al-nanoparticles and tested for ESD ignition. Also, the composites of porous gels were loaded with AAMCAB polymer and mixed with CTBN coated Al-nanoparticles were tested to determine their ESD ignition energy. The following tables provide the results obtained on various composites.

Fe_2O_3 sol-gel + Al (80 nm) ESD Energy, mJ

Voltage Level	Capacitance Value						
	300	450	600	1200	2400	10,000	20,000
	3.13E-10	4.45E-10	5.98E-10	1.30E-09	2.50E-09	1.01E-08	2.00E-08
500	0.04	0.06	0.07	0.16	0.31	1.26	2.50
1000	0.16	0.22	0.30	0.65	1.25	5.05	10.00
1500	0.35	0.50	0.67	1.46	2.81	11.36	22.50
2000	0.63	0.89	1.20	2.60	5.00	20.20	40.00
2500	0.98	**1.39**	1.87	4.06	7.81	31.56	62.50
3000	1.41	2.00	2.69	5.85	11.25	45.45	90.00
3500	1.92	2.73	3.66	7.96	15.31	61.86	122.50
4000	2.50	3.56	4.78	10.40	20.00	80.80	160.00
4500	3.17	4.51	6.05	13.16	25.31	102.26	202.50
5000	3.91	5.56	7.48	16.25	31.25	126.25	250.00

***All energies are in mJ**

Table 5.14: ESD energy values for Fe_2O_3 sol-gel + Al (80 nm)

Fe_2O_3 Sol-gel + Al (115 nm) ESD Energy, mJ

Voltage Level	Capacitance Value						
	300	450	600	1200	2400	10,000	20,000
	3.13E-10	4.45E-10	5.98E-10	1.30E-09	2.50E-09	1.01E-08	2.00E-08
500	0.04	0.06	0.07	0.16	0.31	1.26	2.50
1000	0.16	0.22	0.30	0.65	1.25	5.05	10.00
1500	0.35	0.50	0.67	1.46	2.81	11.36	22.50
2000	0.63	0.89	1.20	2.60	5.00	20.20	40.00
2500	0.98	1.39	1.87	4.06	7.81	31.56	62.50
3000	1.41	2.00	2.69	5.85	11.25	45.45	90.00
3500	1.92	2.73	3.66	7.96	15.31	61.86	122.50
4000	2.50	3.56	4.78	10.40	20.00	80.80	160.00
4500	3.17	4.51	6.05	13.16	25.31	102.26	202.50
5000	3.91	5.56	7.48	16.25	31.25	126.25	250.00

***All energies are in mJ**

Table 5.15: ESD energy values for Fe_2O_3 Sol-gel + Al (115 nm)

Fe_2O_3 Sol-gel + Al (115 nm) 10% CTBN ESD Energy, mJ

Voltage Level	Capacitance Value						
	300	450	600	1200	2400	10,000	20,000
	3.13E-10	4.45E-10	5.98E-10	1.30E-09	2.50E-09	1.01E-08	2.00E-08
500	0.04	0.06	0.07	0.16	0.31	1.26	2.50
1000	0.16	0.22	0.30	0.65	1.25	5.05	10.00
1500	0.35	0.50	0.67	1.46	2.81	11.36	22.50
2000	0.63	0.89	1.20	2.60	5.00	20.20	40.00
2500	0.98	1.39	1.87	4.06	7.81	31.56	62.50
3000	1.41	2.00	2.69	5.85	11.25	45.45	90.00
3500	1.92	2.73	3.66	7.96	15.31	61.86	122.50
4000	2.50	3.56	4.78	10.40	20.00	80.80	160.00
4500	3.17	4.51	6.05	13.16	25.31	102.26	202.50
5000	3.91	5.56	7.48	16.25	31.25	126.25	250.00

***All energies are in mJ**

Table 5.16: ESD energy values for Fe_2O_3 Sol-gel + Al (115 nm) 10% CTBN

Fe_2O_3 Sol-gel+ Al (120 nm) 10% CTBN Coated ESD Energy, mJ

Voltage Level	Capacitance Value						
	300	450	600	1200	2400	10,000	20,000
	3.13E-10	4.45E-10	5.98E-10	1.30E-09	2.50E-09	1.01E-08	2.00E-08
500	0.04	0.06	0.07	0.16	0.31	1.26	2.50
1000	0.16	0.22	0.30	0.65	1.25	5.05	10.00
1500	0.35	0.50	0.67	1.46	2.81	11.36	22.50
2000	0.63	0.89	1.20	2.60	5.00	20.20	40.00
2500	0.98	1.39	1.87	4.06	7.81	31.56	62.50
3000	1.41	2.00	2.69	5.85	11.25	45.45	90.00
3500	1.92	2.73	3.66	7.96	15.31	61.86	122.50
4000	2.50	3.56	4.78	10.40	20.00	80.80	160.00
4500	3.17	4.51	6.05	13.16	25.31	102.26	202.50
5000	3.91	5.56	7.48	16.25	31.25	126.25	250.00

*All energies are in mJ

Table 5.17: ESD energy values for Fe_2O_3 Sol-gel+ Al (120 nm) 10% CTBN Coated

Fe_2O_3 Sol Gel + 5% AAMCAB+Al (115 nm) ESD Energy, mJ

Voltage Level	Capacitance Value						
	300	450	600	1200	2400	10,000	20,000
	3.13E-10	4.45E-10	5.98E-10	1.30E-09	2.50E-09	1.01E-08	2.00E-08
500	0.04	0.06	0.07	0.16	0.31	1.26	2.50
1000	0.16	0.22	0.30	0.65	1.25	5.05	10.00
1500	0.35	0.50	0.67	1.46	2.81	11.36	22.50
2000	0.63	0.89	1.20	2.60	5.00	20.20	40.00
2500	0.98	1.39	1.87	4.06	7.81	31.56	62.50
3000	1.41	2.00	2.69	5.85	11.25	45.45	90.00
3500	1.92	**2.73**	3.66	7.96	15.31	61.86	122.50
4000	2.50	3.56	4.78	10.40	20.00	80.80	160.00
4500	3.17	4.51	6.05	13.16	25.31	102.26	202.50
5000	3.91	5.56	7.48	16.25	31.25	126.25	250.00

***All energies are in mJ**

Table 5.18: ESD energy values for Fe_2O_3 Sol Gel + 5% AAMCAB+Al (115 nm)

Fe_2O_3 Sol Gel + 5% AAMCAB+2.5%CTBN COATED Al (115 nm) ESD Energy, mJ

Voltage Level	Capacitance Value						
	300	450	600	1200	2400	10,000	20,000
	3.13E-10	4.45E-10	5.98E-10	1.30E-09	2.50E-09	1.01E-08	2.00E-08
500	0.04	0.06	0.07	0.16	0.31	1.26	2.50
1000	0.16	0.22	0.30	0.65	1.25	5.05	10.00
1500	0.35	0.50	0.67	1.46	2.81	11.36	22.50
2000	0.63	0.89	1.20	2.60	5.00	20.20	40.00
2500	0.98	1.39	1.87	4.06	7.81	31.56	62.50
3000	1.41	2.00	2.69	5.85	11.25	45.45	90.00
3500	1.92	**2.73**	3.66	7.96	15.31	61.86	122.50
4000	2.50	3.56	4.78	10.40	20.00	80.80	160.00
4500	3.17	4.51	6.05	13.16	25.31	102.26	202.50
5000	3.91	5.56	7.48	16.25	31.25	126.25	250.00

***All energies are in mJ**

Table 5.19: ESD energy values for Fe_2O_3 Sol Gel + 5% AAMCAB+2.5%CTBN coated Al (115 nm)

Fe_2O_3 Sol-gel+5%AAMCAB+ Al (120 nm) 10% CTBN Coated ESD Energy, mJ

Voltage Level	Capacitance Value						
	300	450	600	1200	2400	10,000	20,000
	3.13E-10	4.45E-10	5.98E-10	1.30E-09	2.50E-09	1.01E-08	2.00E-08
500	0.04	0.06	0.07	0.16	0.31	1.26	2.50
1000	0.16	0.22	0.30	0.65	1.25	5.05	10.00
1500	0.35	0.50	0.67	1.46	2.81	11.36	22.50
2000	0.63	0.89	1.20	2.60	5.00	20.20	40.00
2500	0.98	1.39	1.87	4.06	7.81	31.56	62.50
3000	1.41	2.00	2.69	5.85	11.25	45.45	90.00
3500	1.92	2.73	3.66	7.96	15.31	61.86	122.50
4000	2.50	3.56	4.78	10.40	20.00	80.80	160.00
4500	3.17	4.51	6.05	13.16	25.31	102.26	202.50
5000	3.91	5.56	7.48	16.25	31.25	126.25	250.00

*All energies are in mJ

Table 5.20: ESD energy values for Fe_2O_3Sol-gel+5%AAMCAB+ Al (120 nm) 10% CTBN Coated

Fe2O3+ Al (120 nm) 10% CTBN Coated and Separated ESD Energy, mJ

Voltage Level	Capacitance Value						
	300	450	600	1200	2400	10,000	20,000
	3.13E-10	4.45E-10	5.98E-10	1.30E-09	2.50E-09	1.01E-08	2.00E-08
500	0.04	0.06	0.07	0.16	0.31	1.26	2.50
1000	0.16	0.22	0.30	0.65	1.25	5.05	10.00
1500	0.35	0.50	0.67	1.46	2.81	11.36	22.50
2000	0.63	0.89	1.20	2.60	5.00	20.20	40.00
2500	0.98	1.39	1.87	4.06	7.81	31.56	62.50
3000	1.41	2.00	2.69	5.85	11.25	45.45	90.00
3500	1.92	2.73	3.66	7.96	15.31	61.86	122.50
4000	2.50	3.56	4.78	10.40	20.00	80.80	160.00
4500	3.17	4.51	6.05	13.16	25.31	102.26	202.50
5000	3.91	5.56	7.48	16.25	31.25	126.25	250.00

*All energies are in mJ

Table 5.21: ESD energy values for Fe_2O_3Sol-gel+5%AAMCAB+ Al (120 nm) 10% CTBN coated phase separated

Table 5.22 summarizes the ESD ignition energy for the porous Fe_2O_3 gel-based composites. The following values show gradual increase in ESD ignition energy when the porous gel modified with the polymer were used. The ESD ignition energy of 31.56 mJ was obtained for the composites prepared with porous gel loaded with 5%AAMCAB and mixed with Al (120 nm) particles coated with 10% CTBN polymer and separated.

Composite Type (Sol-gel)	**ESD Ignition Energy (mJ)**
Fe_2O_3 Sol-gel + Al (80 nm)	1.39
Fe_2O_3 Sol-gel + Al (115 nm)	1.39
Fe_2O_3 Sol-gel + Al (115 nm) 10% CTBN	11.36
Fe_2O_3 Sol- gel + 5% AAMCAB+Al (115 nm)	2.73
Fe_2O_3 Sol-gel+5% AAMCAB +2.5% CTBN coated Al (115 nm)	2.73
Fe_2O_3 Sol-gel+5%AAMCAB+ Al (120 nm) 10% CTBN coated	20.20
Fe_2O_3 Sol-gel+5%AAMCAB+ Al (120 nm) 10% CTBN coated phase separated	31.56

Table 5.22 ESD ignition values for Fe_2O_3 gel-based composites

CONCLUSION

Ordered porous Fe_2O_3 gel has been successfully synthesized using surfactant templating method. Combustion wave velocities of porous gel-based energetic composites were measured and compared with particle-based composites. The former shows lower rates of combustion as compared with the latter. The pressure vs. time profile indicates that the particle-based composites do not sustain pressure for longer times, whereas for gel-based composites a pressure of 2.3 MPa obtained from 200 mg materials sustains for a period of more than 40 ms. The possible reason for pressure sustenance is due to the diffusion resistance for the gases produced on combustion of polymer inside nanosized porous confinements. Thus it is concluded that gel-based composites have superior propellant characteristics as compared with particle-based composites. The polymers employed in improving the performance of porous gels also increase ESD ignition energy, which is highly desirable for usage and handling of the nanoenergetic composites in a safe manner. The composite of nanoporous Fe_2O_3 gel modified with 5% AAMCAB polymer and mixed with Al-nanoparticles (120 nm) coated with 10% CTBN polymer and separated has been found to have combustion wave speed of 38 m/s, pressure sustenance over a period of more than 40 ms, and ESD ignition energy of 45.5 mJ, which will be highly useful for propellant applications.

FUTURE WORK

The results obtained in the preceding chapters indicate that it is possible to manipulate nano composite materials for a desired effect. It is also seen that it will be possible to inhibit and limit the electrostatic ignition energy of the nano composites using polymers. The following studies can be done in the future:

1. Study the ignition energy sensitivity in the context of voltages and capacitances, i.e. it is noted that the nano composite has less sensitivity for capacitances as compared to voltages for the same energy.
2. Studying the characteristics of nano composites using different polymers.
3. Finding a technique to make sure that each of the nano particles is coated. Though the technique of phase separation helps to some extent, it is not sure if it can be used for all metal powders.
4. Making sure the coating does not wear off while handling.

Though one could think of many avenues to work in this area, it would mostly depend on the type of use and parameters needed for a specific application. Needless to say, the field of nano technology is going to find many uses in the future.

REFERENCES

1. Aero-Sol-Gel synthesis of nanoporous Iron-Oxide particles: A Potential oxidizer for nanoenergetic materials - Anand Prakash, Alon V. McCormick and Michael R. Zachariah Departments of Mechanical and Chemical Engineering University of Minnesota. Chem. Mater.2004, 16, 1466-1471.
2. Combustion wave speeds of nanocomposite Al/Fe2O3: the effects of Fe2O3 particle synthesis technique - Keith B. Plantier, Michelle L. Pantoya, Alexander E. Gash.
3. Basics of Static Electricity: Sources, Damage, Prevention – SSC Technical Bulletin.
4. Electro-Static Discharge - Thermionic Incorporated Technical Bulletin.
5. Combustion and reaction propagation of four nano scale energetic composites – V. Eric Sanders, Blaine W. Asay, Timothy J. Foley, Bryce C. Tappan, Adam M. Pacheco and Steven M. Son, Las Alamos laboratory, NM, 87545.
6. Formation of Nanostructured Energetic materials via Modified Sol-gel synthesis - Jeremy Walker and Rina Tannenbaum. Mat. Res.Soc.Symp.Proc.Vol.800© 2004 Material Research society.
7. Ferrihydrite gels derived in the $Fe(NO_3)_3.9H_2O$-C_2H_5OH-CH_3CHCH_2O ternary systems - Evgueni F. Talatsev, Michelle L. Pantoya, Cristina Camagong, Bashar Lahlouh, Steven M. Nicolich, Shubhra Gangopadhyay. Journal of Non-crystalline Solids 351(2005) 1426-1432.
8. http://homepages.cae.wisc.edu/~aerogel/aboutaerogel.html
9. Nanocatalysts for reactions in supercritical carbon dioxide, IRF 03-026, Idaho Research Foundation, Inc.
10. Synthesis of ordered nanoporous composites- A Thesis presented to the faculty of Graduate School University of Missouri-Columbia by Mehendale Bhushan. J, May 2005
11. Propellant Chemistry - Patrick Foley and Peter Mader. CHIMIA 2004, 58 No. 6.
12. Chemical approaches to the synthesis of Inorganic materials – C.N.R. Rao, Chapter 8, Sol-gel synthesis. John Wiley & Sons (PTE) Limited.

13. Energetic Nanocomposites with sol-gel chemistry: Synthesis, Safety, and Characterization - A.E Gash, R.L. Simpson, J.H. Satcher,Jr. Article submitted to 29th International Pyrotechnic Seminar, Westminster,CO., July14-19, 2002.
14. Nanoenergetic composite of mesoporous iron oxide and aluminum nanoparticles - Bhushan Mehendale, Rajesh Shende, Senthil Subramanian, Paul Redner, Deepak Kapoor, Steven Nicolich, , and Shubhra Gangopadhyay
15. Nanocrystalline Iron Oxide Aerogels as Mesoporous Magnetic Architectures - Jeffrey W. Long, Michael S .Logan, Christopher P. Rhodes, Everett E. Carpenter, Rhonda M. Stroud, and Debra R. Rolison. J.A.C.S Articles, Published on web 12/04/2004
16. www.sigmaaldrich.com
17. http://depts.washington.edu/solgel/images/courses/MSE_502/Ch_2/figure 2.18 JPG.
18. Enhancing the rate of energy release from nanoenergetic materials by electrostatically enhanced assembly – Soo H. Kim, Michael R. Zachariah – Adv. Matter. 2004, 16, No. 20, October 18.
19. A Novel On-Chip diagnostic Method to Measure Burn Rates of Energetic Materials - Shantanu Bhattacharya, Yuanfang Gao, Steven Apperson, Senthil Subramaniam, Rajesh Shende, Evgueni Talantsev.
20. Firing test system model 931, operating manual - electro-tech systems, inc.
21. S. Gangopadhyay, R.V. Shende, Yuanfang Gao, S. Bhattacharya, S. Hasan. S.Apperson, S. Subramanian, M.Hossain, US patent, 2005 (in progress).
22. AIAA-2004-3549,NASA/TM-2004-213211 - J.D. Wrbanek, G.C. Fralick, S.C.Farmer, A. Sayir, C.A. Blaha, J.M. Gonzalez.
23. Detonation: Theory and Experiment - Dover publication, Inc., New York, 1979. Fickett, W and Davis, W.C.
24. International Annual conference of ICT(2005) 36th (Energetic Material), 110, 1-11 - Laritchev, I. Leipunsky, O. Laricheva, P. Pshechenkov, J. Pavel, K. Alexey, V. Sedoi.

25. Surface Characterization of Energetic Materials using Point-to-point Contact FTIR-ATR - Joyce Newberry, Pamela J. Kaste, IEEE Transactions on Magnetics, Vol.39, NO.1, January 2003.
26. Sonochemical Synthesis of Mesoporous Iron Oxide and accounts of its Magnetic and Catalytic Properties - D.N. Srivastava, N.Perkas, A.Gedanken and I. Felner. J. Phys.Chem.B 2002, 106, 1878-1883.
27. Modeling of Electrostatic Fields in solid propellants using finite element techniques - Vivek R.D. Sunderraj, John D. Curry, and Ronal W. Larson.
28. Sonochemistry as a tool for preparation of porous metal oxides - Srivastava, D. N.; Perkas, N.; Zaban, A.; Gedanken, A. Department of Chemistry, Bar-Ilan University, Ramat-Gan, Israel. Pure and Applied Chemistry (2002), 74(9), 1509-1517. CODEN: PACHAS ISSN: 0033-4545. Journal; General Review written in English. CAN 138:45085 AN 2002:841463 CAPLUS (Copyright 2005 ACS on SciFinder (R)).
29. Two and three-dimensional mesoporous Iron oxides with microporous walls – Feng Jiao and peter G. Bruce. Agnew. Chem..int. ed. 2004, 43-5958-5961.
30. Nanostructured materials processing, diagnostics and modeling – A presentation by Michael R. Zachariah - Particle technology laboratory, Department of mechanical engineering and chemistry, University of Minnesota.
31. Surfactant assisted synthesis of alumina with hierarchical nanoporews - Weihua Deng, Michael W. Toepke, and Brent H. Shanks- Advanced functional materials. 2003, 13, No. 1, January.
32. Micro-Raman investigation of iron oxide films and powders produced by sol-gel synthesis – D. Bersani, P.P. Lottici and A. Montenero. Journal of Raman spectroscopy, 30, 355-360 (1999).
33. Use of Epoxides in the Sol-Gel synthesis of porous iron(III) oxide Monoliths from Fe(III) salts - Alexander E. gash, Thomas M.Tilloston, Joe H.Satcher,Jr., John F.Poco, Lawrence W. Hrubesh and Randall L. Simpson. Chem. Mater. 2001, 13, 999-1007.
34. Nanostructured materials and nanotechnology - Edited by – Hari Singh Nalwa-Chapter1&2.

35. Nanotechnology - Editor- Gregory Timp.
36. Hazard characterization of aluminum nano powder composition - David. E. G. Jones, Richard Turcotte, Richard C. Fouchard, Queenie S.M. Kwok, Ann-Marie Turcotte and Zainab Abdel-Qader- Propellants, Explosives, pyrotechnics 28 (2003), No 3.
37. Solid propellant microrockets - Dana Teasdale- Research project submitted to the department of electrical engineering and computer science, University of California, Berkely, 19th, may 2000.
38. Nanocrystalline Iron oxide Aerogels and mesoporous magnetic architecture – Jeffrey W. Long, Michael S. Logan, Christopher P. Rhodes, Everett E. Carpenter, Rhonda M. Stroud and Debra R. Rolison. J.Am. Chem .Soc. 2004. 126. 16879-16889.